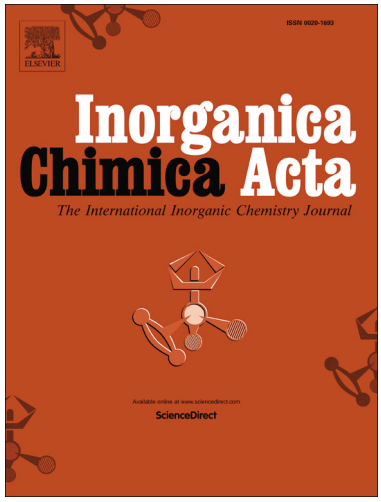

Research paper

A Ru(II)-*p*-cymene compound bearing naproxen-pyridineamide. Synthesis, spectroscopic studies, computational analysis and *in vitro* anticancer activity against lung cells compared to Ru(II)-*p*-cymene-naproxen and the corresponding drug ligands

Julie Pauline Gaitan Tabares, Rodrigo Luis S.R. Santos, Jefferson Luiz Cassiano, Marcio H. Zaim, João Honorato, Alzir A. Batista, Sarah F. Teixeira, Adilson Kleber Ferreira, Rommel B. Viana, Sandra Quispe Martínez, Antonio Carlos Stábile, Denise de Oliveira Silva

PII: S0020-1693(18)31792-4
DOI: https://doi.org/10.1016/j.ica.2019.01.030
Reference: ICA 18753

To appear in: *Inorganica Chimica Acta*

Received Date: 2 December 2018
Revised Date: 25 January 2019
Accepted Date: 25 January 2019

Please cite this article as: J.P.G. Tabares, R.L.S.R. Santos, J.L. Cassiano, M.H. Zaim, J. Honorato, A.A. Batista, S.F. Teixeira, A.K. Ferreira, R.B. Viana, S.Q. Martínez, A.C. Stábile, D. de Oliveira Silva, A Ru(II)-*p*-cymene compound bearing naproxen-pyridineamide. Synthesis, spectroscopic studies, computational analysis and *in vitro* anticancer activity against lung cells compared to Ru(II)-*p*-cymene-naproxen and the corresponding drug ligands, *Inorganica Chimica Acta* (2019), doi: https://doi.org/10.1016/j.ica.2019.01.030

A Ru(II)-*p*-cymene compound bearing naproxen-pyridineamide. Synthesis, spectroscopic studies, computational analysis and *in vitro* anticancer activity against lung cells compared to Ru(II)-*p*-cymene-naproxen and the corresponding drug ligands

Julie Pauline Gaitan Tabares [a], Rodrigo Luis S. R. Santos [a,b], Jefferson Luiz Cassiano [a], Marcio H. Zaim [c], João Honorato [d], Alzir A. Batista [d], Sarah F. Teixeira [e], Adilson Kleber Ferreira [e], Rommel B. Viana [f, 1], Sandra Quispe Martínez [a], Antonio Carlos Stábile [a], Denise de Oliveira Silva [a, *]

[a] Laboratory for Synthetic and Structural Inorganic Chemistry - Bioinorganic and Metallodrugs. Department of Fundamental Chemistry, Institute of Chemistry, University of São Paulo. Av. Prof. Lineu Prestes, 748, 05508-000, São Paulo, SP, Brazil.

[b] Department of Exact and Technological Sciences, State University of Santa Cruz. Rod. Jorge Amado, Km 16, 45662-900, Ilhéus, BA, Brazil.

[c] Catalysis and Transfer Phase Laboratory. Department of Fundamental Chemistry, Institute of Chemistry, University of São Paulo. Av. Prof. Lineu Prestes, 748, 05508-000, São Paulo, SP, Brazil.

[d] Department of Chemistry, Federal University of São Carlos, CP 676, 13565-905, São Carlos, SP, Brazil.

[e] Department of Immunology. Laboratory of Tumor Immunology. Institute of Biomedical Sciences, University of São Paulo. Av. Prof. Lineu Prestes, 1730, 05508-000, São Paulo, SP, Brazil.

[f] Departament of Chemistry and Molecular Physics, São Carlos Chemistry Institute, University of São Paulo. Av. Trabalhador São Carlense, 400, 13566-590, São Carlos, SP, Brazil.

[*]Corresponding author: *Email address*: deosilva@iq.usp.br (D. de Oliveira Silva).

[1] Current address: Chemistry Institute, Federal University of Alfenas, MG, Brazil.

Abstract

The design of new Ru(II) organometallics is a subject of interest to the field of anticancer metallodrugs. This work reports the interaction of the Ru(II)-η^6-*p*-cymene framework with the naproxen-pyridineamide (Npxpya, **L1**), a structurally modified form of the naproxen (HNpx, **HL2**) drug, to give the new organometallic [Ru(η^6-*p*-cymene)(**L1**)Cl_2] **(1)** bearing the Npxpya ligand. The reported naproxenate derived, [Ru(η^6-*p*-cymene)(**L2**)Cl] **(2)**, is re-prepared also from the precursor [Ru(η^6-*p*-cymene)Cl_2]$_2$ **(3)** and additional investigation is performed. The **L1** ligand and the two Ru(II)-arenes are fully characterized by ESI-MS, NMR, ATR/FT-IR and UV/VIS, and their structures corroborated by DFT computational calculations. Time-dependent ^{1}HMNR studies show that both Ru(II)-arenes, despite being stable in non-coordinating solvents, undergo distinct step dissociation in dimethylsulfoxide solvent to give the corresponding drug ligands and [Ru(η^6-*p*-cymene)dmsoCl_2] **(4)** species. Experimental electronic absorption spectroscopy data show good correlation with DFT calculations. Organometallics **1** and **2** as well as their corresponding parent drug ligands exhibit luminescence properties mainly associated to the naproxen moiety. Screening in NCI-H460 and A549 lung cancer cells reveals lack of activity of **2** and **L2** while the new organometallic **1** is found to inhibit cell proliferation of both types of cell lines in similar way to the free **L1**. The structural modification, by the insertion of the pyridineamide moiety into the original structure of naproxen, to form the Npxpya conjugated drug, is shown to be crucial for the anticancer activity. Compound **1**, in similar way to species **4** (generated from dissolution of **3** in dmso), and despite having IC_{50} close to the IC_{50} of **L1**, does not show significant effect on the mitochondrial membrane potential (MMP), in contrast to the behavior of the **L1** parent free drug which significantly decreases the MMP in NCI-H460 cells. Interestingly, since ^{1}HMNR studies indicate that organometallic **1** is completely dissociated in dmso (the solvent used to prepare the drug solutions for cell treatment in the biological assays) to give the **L1** free drug and species **4**, it is plausible to infer that the presence of Npxpya-free Ru species, probably in the form of species **4**, might play a role in inhibiting the mechanism related to the mitochondrial function when cells are treated with **1**, in comparison with the cell treatment with the free **L1**.

Keywords: Ruthenium(II) organometallics, *p*-cymene, naproxen, naproxen-pyridineamide, metallodrug.

1. Introduction

The investigation of chemical and biological properties of potential metallodrugs play key role in the development of new antitumor agents aiming to broad strategies targeting cancer therapy. The early success of platinum chemotherapeutics yet accompanied by severe limitations in the clinical treatment of cancer led to an extensive search for non-platinum drugs which pointed to the promising anticancer activity of diverse ruthenium compounds [1-18].

An interesting approach to the development of new pharmaceuticals is the design of drugs in which metal ions are combined with bioactive compounds already used in clinic. In this context, the non-steroidal anti-inflammatory drugs (NSAIDs) that are widely prescribed to treat pain, fever and inflammation, and also show antitumor properties, constitute a unique class of pharmaceuticals to be explored [19-23]. In fact, NSAIDs have been successfully used to build metal-based drugs which may show enhanced efficacy and/or reduced side-effects in relation to the correspondent organic parent drugs [3,5,24,25]. Carboxylic NSAIDs have been used for many years in de Oliveira Silva's scientific research to develop new metallo-NSAIDs [3,5,26-29]. In particular, a unique class of metallodrugs bearing metal-metal multiply bonded Ru_2(II,III) cores stabilized by four NSAID-derived carboxylate ligands was successfully designed. The combination of the dimetal core and the NSAIDs in $[Ru_2(O_2CR)_4]^+$ paddlewheel type structured units succeeded in promoting synergistic effects leading to the enhancement of *in vitro* and *in vivo* anticancer activity [30-36].

It is noteworthy that the growth in the field of ruthenium-based drugs has been driven in part by the early promising results from phase trials conducted for the well-known antimetastatic NAMI-A, (Him)[*trans*-$RuCl_4$(dmso)im], im = imidazole [37,38], and the structurally related cytotoxic KP1019, (Hind)[*trans*-$[RuCl_4(ind)_2]$, ind = indazole, which was further replaced by the more stable sodium salt NKP1339 in the clinical trials [39,40]. The expansion of the ruthenium-based drugs is also clearly marked by the development of a number of Ru(II) organometallics to which good activity against primary or metastatic tumors, and lower cytotoxicity than platinum drugs, have been attributed [13,41,42]. Particular attention has been given to organometallics in which three of the coordination sites are occupied by a η^6-coordinated arene stabilizing the Ru(II) oxidation state. Two well-known representatives of families of these compounds are RAPTA-C, ($[Ru(\eta^6$-*p*-cymene)(pta)$Cl_2]$, pta = 1,3,5-triaza-7-phosphatricyclo[3.3.1.1]decane, and RAED-C, ($[Ru(\eta^6$-*p*-cymene)(en)Cl][PF_6]), en = ethylenediamine), both of them bearing the *p*-cymene (cym)

ligand [43,44]. More recently, NSAIDs and derivatives has attracted attention as ligands also in the field of ruthenium organometallics aiming the study of anticancer properties [45,46].

In this context, we have investigated here the interaction of the Ru(II)-η^6-*p*-cymene framework with the naproxen-pyridinenamide (Npxpya, **L1**, or *5-N-*4*(*Pyridyl)-2-(6-methoxy-2-naphthyl)propionamide), a structurally modified form of the naproxen (HNpx or **HL2**) drug carrying a moiety from the biologically active 4-aminopyridine [47-50]. Naproxen, besides being currently used to treat rheumatic and arthritis diseases [51], exhibits activity against cancer and viral diseases as well as some of its derivatives [52-58] and, moreover, it has been reported as typical photoactive drug [59-62]. No studies reporting biological activity or applications as a ligand in metal complexes were found for the modified drug in the form of Npxpya, although this compound is claimed as a reagent for resolution of racemic mixtures of optically derivatives of cyclopropane [63].

In this work, we report for the first time the synthesis and characterization of the new organometallic [Ru(η^6-*p*-cymene)(**L1**)Cl_2] **(1)** and an alternative synthetic route for Npxpya (**L1)**. We have also re-prepared and performed additional investigation for the naproxenate-derived [Ru(η^6-*p*-cymene)(**L2**)Cl] **(2)** which was previously reported [64]. The compounds are characterized by ESI-MS, NMR, ATR/FT-IR and UV/VIS, and their structures corroborated by DFT computational calculations. Photophysical properties and biological activity against NCI-H460 and A549 lung cancer cell lines are described.

2. Experimental

2.1 Reagents and solvents

Reagents from Sigma-Aldrich or Merck were used without further purification. Solvents from Merck or LabSynth were dried by standard methods. Deuterated solvents ($CDCl_3$, *d*-methanol (*d*-MeOH), and *d*-dmso) were from Sigma-Aldrich. Naproxen (HNpx or **HL2**) was purchased from manipulation pharmacy (Purifarma) in São Paulo, Brazil, and characterized by ^{1}H NMR (Appx. SM.1.1). The sodium naproxenate salt (**NaL2**) was prepared from neutralization reaction between **HL2** and NaOH, and characterized by ^{1}H NMR and ATR-FTIR (Appx. SM.1.2). The syntheses of the Ru(II)-arene compounds were carried out under nitrogen atmosphere using standard Schlenk techniques. Precursor [Ru(η^6-*p*-cymene)Cl_2]$_2$ **(3)** (Figure 1) was synthesized by a method adapted from the literature [65], and characterized by ^{1}H NMR, ATR-FTIR, UV/VIS (Appx. SM.1.3). The dmso-derived compound, [Ru(η^6-*p*-cymene)dmsoCl_2] **(4)** (Figure 1), was prepared by a method adapted from the literature [66], and characterized by ^{1}H NMR (Appx. SM.1.4).

2.2. Syntheses

2.2.1 Npxpya (L1)

The 4-aminopyridine (0.96 g; 0.01 mol) was added to a mixture of **HL2** (2.34 g; 0.01 mol) and DCC (N,N'-dicyclohexylcarbodiimide, 2.66 g; 0.013 mol) that has been previously stirred for 1-2 min in CH_2Cl_2 (60 mL). This solution was stirred overnight at room temperature, and then it was filtered to remove small amounts of solid impurities (excess DCC and residual DCU dicyclohexylurea). To purify the product from more of these impurities, the filtrate was kept under refrigeration until more solid was formed, and then submitted to filtration again. This purification procedure (refrigeration/filtration) was repeated until no more solid was precipitated. The final filtrate was roto-evaporated and purified by column chromatography (silica gel Merck, 2.6 x 30 cm, 0.063-200 mm; ethyl acetate as eluent), accompanied by thin layer chromatography (TLC, silica gel) analysis. The purified fraction collected from the chromatography column had the volume reduced to dryness by roto-evaporation. Yield 91 %. Anal. calc. (%) for $C_{19}H_{18}O_2N_2 \cdot 1/2\ H_2O$: C, 72.3; H, 6.07; N, 8.89. Found: C, 71.99; H, 5.92; N, 9.00. **ESI-MS(+)**, CH_2Cl_2/MeOH (m/z): 307.14, $[\mathbf{L1}+H]^+$ requires 307.14; 329.13, $[\mathbf{L1}+Na]^+$ requires 329.13. **^{1}H NMR**, 500 MHz, $CDCl_3$, δ (ppm *vs* TMS), Appx. SM.2, Fig. S1a: 8.40 (dd, $^3J_{H\text{-}H}$ = 4.9, $^4J_{H\text{-}H}$ = 1.5 Hz, 2H, CH_{py} *1*); 7.76 (d, $^3J_{H\text{-}H}$ = 8.5 Hz, 1H, CH_{ring} *10*); 7.72 (d, $^3J_{H\text{-}H}$ = 9.0 Hz, 1H, CH_{ring} *7*); 7.70 (d, $^4J_{H\text{-}H}$ = 1.5 Hz, 1H, CH_{ring} *6*); 7.40 (dd, $^3J_{H\text{-}H}$ = 8.5 Hz, $^4J_{H\text{-}H}$ = 1.8 Hz 1H, CH_{ring} *11*); 7.36 (dd, $^3J_{H\text{-}H}$ = 4.8, $^4J_{H\text{-}H}$ = 1.6 Hz, 2H, CH_{py} *2*); 7.18 (dd, $^3J_{H\text{-}H}$ = 8.9 Hz, $^4J_{H\text{-}H}$ =2.5 Hz 1H, CH_{ring} *8*); 7.14 (d, $^4J_{H\text{-}H}$ = 2.5 Hz, 1H, CH_{ring} *9*); 3.92 (s, 3H, O-CH_3 *12*); 3.86 (q, $^3J_{H\text{-}H}$ = 7.1 Hz, 1H, CH_{chiral} *4*); 1.66 (d, $^3J_{H\text{-}H}$ = 7.1 Hz, 3H, C_{chiral}-CH_3 *5*). **^{13}C NMR** (500 MHz, $CDCl_3$, δ (ppm), Appx. SM.2, Fig. S1b: 173.26 (***C***=O); 158.01 (***C***-OCH_3); 150.48 (N_{py}-***C***H); 145.03 (HN-***C***$_{py}$); 135.27 (C_{chiral}-***C***$_{ring}$); 133.99 (***C***$_{ring}$), 129.22 (***C***H$_{ring}$), 128.99 (***C***$_{ring}$), 128.06 (***C***H$_{ring}$), 126.40 (***C***H$_{ring}$), 125.85 (***C***H$_{ring}$); 119.52 (***C***H$_{ring}$); 113.41 (***C***H$_{py}$); 105.70 (***C***H$_{ring}$); 55.37 (O-***C***H$_3$); 48.20 (***C***H$_{chiral}$); 18.48 (C_{chiral}-***C***H_3). **ATR-FTIR** major bands, ν(cm^{-1}): 3322w, 3251w, 3160w, 3066w (pya νNH); 3000sh, 2975w,2930w,2866w (Npx νCH); 1702vs (pya νC=O); 1589s (pya N-H bending); 1506s (pya νCN_{ring} + νCC_{ring} and Npx δCH_3); 1416s (pya ν_{ring}); 1336m,1323sh (pya νCN_{ring}); 1400-1370w (Npx CH_3 rocking); 1284s (pya νCN_{ring}); 1264s (Npx *in plane* CC_{ring} deformation); 1227s,1209sh,1181s (pya νCC_{ring} and Npx *in plane* CH_{ring} bending + CH_3 rocking); 1181s (pya νCC_{ring}); 1070w,1051w,1029w,997w (pya ring breathing and Npx

bands; 900-800w, 778m (pya *out of plane* CH_{ring} bending). **UV/VIS**, λ_{max} (nm) / ε ($mol^{-1}Lcm^{-1}$): 275(sh)/ n.d.; 285(sh)/ 5000; 318/ 1800; 333/2000 (in CH_2Cl_2).

2.2.2 [Ru(η^6-*p*-cymene)(L1)Cl$_2$] (1) (Figure 1)

Compound **3** (0.10 g; 0.16 mmol) and **L1** (0.098 g; 0.32 mmol) were stirred in CH_2Cl_2 (15 mL) for 5 h, at room temperature. After removal of the solvent on a rotary evaporator, the residue was dissolved in minimum amount of acetone and then precipitated with addition of hexane. The product was washed with portions of hexane and dried in vacuum to give an orange solid. Yield 71 %. Anal. calc. (%) for $C_{29}H_{32}N_2O_2ClRu$: C, 56.86; H, 5.26; N, 4.57; Cl, 11.57. Found: C, 56.52; H, 5.25; N, 4.75; Cl, 10.65. **ESI-MS(+)**, $CHCl_3/CH_3CN$ (m/z): 577.12, [Ru(cym)(**L1**)Cl]$^+$ requires 577.12; 541.14, [Ru(cym)(**L1**)-1H]$^+$ requires 541.14; 270.98, [Ru(cym)Cl]$^+$ requires 270.98. **^{1}H NMR**, 300 MHz, $CDCl_3$, δ (ppm *vs* TMS), Appx. SM.3, Fig. S2a: 7.93-7.83 (m, 3H and 2H, Npxpya CH_{ring} *6,7,10* and Npxpya CH_{py} *1*; 7.61 (d, $^3J_{H\text{-}H}$ = 8.1 Hz, 1H, Npxpya CH_{ring} *11*); 7.20 – 7.17 (m, 2H, Npxpya CH_{ring} *8,9*); 6.96 (d, $^3J_{H\text{-}H}$ = 6.3 Hz, 2H Npxpya CH_{py} *2*); 5.36 (d, $^3J_{H\text{-}H}$ = 5.7 Hz, 1H, cym CH*b*); 5.01 (d, $^3J_{H\text{-}H}$ = 5.7 Hz, 1H, CH*a*); 4.10 (q, $^3J_{H\text{-}H}$ = 6.8 1H, Npxpya CH_{chiral} *4*); 3.92 (s, 3H, Npxpya O-CH_3 *12*); 2.81 (m, $^3J_{H\text{-}H}$ = 6.8, 1H, cym CH*c*-$(CH_3)_2$); 1.77 (s, 3H, cym CH_3 *d*); 1.57 (d, $^3J_{H\text{-}H}$ = 6.7 Hz, 3H, Npxpya C_{chiral}-CH_3 *5*); 1.24 (dd, $^3J_{H\text{-}H}$ = 6.8, 6H, cym CH(CH_3*e*)$_2$). **^{13}C NMR**, 500 MHz, $CDCl_3$, δ (ppm), Appx. SM.3, Fig. S2b: 173.91 (***C***=O); 157.64 (Npxpya ***C***-OCH_3); 154.13 (Npxpya N_{py}-***C***H); 146.42 (Npxpya HN-***C***$_{py}$); 136.12 (Npxpya C_{chiral}-***C***$_{ring}$); 133.81 (Npxpya ***C***$_{ring}$); 129.43 (Npxpya ***C***H_{ring}), 128.88 (Npxpya ***C***$_{ring}$); 127.28 (Npxpya ***C***H_{ring}); 127.13 (Npxpya ***C***H_{ring}); 126.42 (Npxpya ***C***H_{ring}), 118.96 (Npxpya ***C***H_{ring}), 115.01 (Npxpya ***C***H_{py}); 105.72 (Npxpya ***C***H_{ring}); 102.98 (cym ***C***$_{ring}$-$(CH(CH_3)_2)$; 96.95 (cym ***C***$_{ring}$-CH_3); 83.39 (cym ***C***H); 83.18 (cym ***C***H); 81.61 (cym ***C***H); 81.24 (cym ***C***H); 55.35 (Npxpya O-***C***H_3); 47.34 (Npxpya ***C***H_{chiral}); 30.60 (cym ***C***H$(CH_3)_2$); 22.27 (cym CH(***C***$H_3)_2$); 22.23 (cym CH(***C***$H_3)_2$); 19.00 (Npxpya C_{chiral}-***C***H_3); 18.04 (cym C_{ring}-***C***H_3). **NMR HSQC/HMBC** (Appx. SM.3, Fig. S3, TS1), **NOESY** (Appx. SM.3, Fig. S4). **ATR-FTIR** major bands, ν(cm^{-1}): 3313vw, 3245w, 3163vw, 3068w (pya νNH); 2964mw, 2932mw, 2873vw, 2847vw (Npx νCH); 1702m (pya νC=O); 1632sh, 1603 sh, 1590s (pya N-H bending); 1502vs (pya νCN_{ring} + νCC_{ring} and Npx δCH_3); 1424m (pya ν$_{ring}$); 1339sh, 1327w (pya νCN_{ring}); 1400-1370w (Npx CH_3 rocking); 1294s (pya νCN_{ring}); 1263s (Npx *in plane* CC_{ring} deformation); 1227w,1209m (pya νCC_{ring} and Npx *in plane* CH_{ring} bending + CH_3 rocking); 1174sh,1181s (pya νCC_{ring}); 1084w,1060w,1027m (pya ring breathing and Npx bands); 853sh, 834m-br, 806sh-m (pya *out of plane* CH_{ring} bending). **UV/VIS**, λ_{max} (nm) / ε ($mol^{-1}Lcm^{-1}$): 280 (sh)/ n.d.; 332/4000; 406/ 800 (in CH_2Cl_2).

2.2.3 [Ru(η^6-*p*-cymene)(L2)Cl] (2) (Figure 1)

Compound **3** (0.10 g, 0.16 mmol) and **NaL2** (0.11 g, 0.42 mmol) were added to deaerated methanol (30 mL) and stirred for 1 h, at room temperature. The solvent was removed on a rotary evaporator and the solid was extracted with CH_2Cl_2. After filtration, the solution was roto-evaporated and the residue was dissolved in small volume of acetone before addition of hexane. The product was washed with portions of hexane and dried in vacuum. Yield 87 %. Anal. calc. (%) for $C_{24}H_{27}ClO_3Ru \cdot H_2O$: C, 55.65; H, 5.64; Cl, 6.84. Found: C, 55.63; H, 5.04; Cl, 6.89. **ESI-MS(+)**, $CHCl_3/CH_3CN$ (m/z): 465.10, $[Ru(cym)(\mathbf{L2})]^+$ requires 465.10; 312.01, $[Ru(cym)(CH_3CN)Cl]^+$, requires 312.01; 270.98, $[Ru(cym)Cl]^+$ requires 270.98. **^{1}H NMR**, 500 MHz, $CDCl_3$, δ (ppm *vs* TMS), Appx. SM.4, Fig. S5a: 7.70-7.65 (m, 3H, Npx CH_{ring} *3,4,7*); 7.40 (dd, $^3J_{H\text{-}H}$ = 8.5, $^4J_{H\text{-}H}$ = 1.6 Hz, 1H, Npx CH_{ring} *8*); 7.14–7.10 (m, 2H, Npx CH_{ring} *5,6*); 5.54 (d, $^3J_{H\text{-}H}$ = 5.8 Hz, 2H, cym CH*b*); 5.32 (d, $^3J_{H\text{-}H}$ = 5.8 Hz, 2H, cym CH*a*); 3.91 (s, 3H, Npx O-CH_3 *9*); 3.52 (q, $^3J_{H\text{-}H}$ = 7.1 Hz, 1H, Npx CH_{chiral} *1*); 2.87 (m, $^3J_{H\text{-}H}$ = 7.0, $^4J_{H\text{-}H}$ = 3.0 Hz, 1H, cym CH*c*-$(CH_3)_2$); 2.29 (s, 3H, cym CH_3 *d*); 1.43 (d, $^3J_{H\text{-}H}$ = 7.2 Hz, 3H, Npx C_{chiral}-CH_3 *2*); 1.27 (m, $^3J_{H\text{-}H}$ = 6.9 Hz, 6H, cym $CH(CH_3e)_2$). **^{13}C NMR**, 500 MHz, $CDCl_3$, δ (ppm vs TMS), Appx. SM.4, Fig. S5b: 193.60 (Npx ***C***OO); 157.50 (Npx ***C***-OCH_3); 135.33 (Npx C_{chiral}-***C***$_{ring}$); 133.63 (Npx ***C***$_{ring}$); 129.31 (Npx ***C***H$_{ring}$); 128.97 (Npx ***C***$_{ring}$); 126.92 (Npx ***C***H$_{ring}$); 126.73 (Npx ***C***H$_{ring}$); 126.24 (Npx ***C***H$_{ring}$), 118.69 (Npx ***C***H$_{ring}$); 105.59 (Npx ***C***H$_{ring}$); 100.73 (cym ***C***$_{ring}$-$(CH(CH_3)_2)$; 94.33 (cym ***C***$_{ring}$-CH_3); 78.13 (cym ***C***H); 77.69 (cym ***C***H); 55.30 (Npx O-***C***H_3); 48.11 (Npx ***C***H$_{chiral}$); 31.48 (cym ***C***H$(CH_3)_2$); 22.27 (cym CH(***C***$H_3)_2$); 18.82 (cym C_{ring}-***C***H_3); 18.09 (Npx C_{chiral}-***C***H_3). **NMR HSQC/HMBC** (Appx. SM.4, Fig. S6, TS2). **ATR-FTIR** major bands, ν(cm^{-1}): 1630w, 1605m (Npx νCC_{ring} + *in plane* CH_{ring} bending); 1505m, 1501sh (Npx and cym δCH_3, cym νCC_{ring}), 1488-1450w (Npx and cym νCC_{ring}); 1460s (Npx ν_aCOO); 1437s (Npx ν_sCOO); 1387-1373w (Npx and cym CH_3 rocking); 1267s (Npx *in plane* CC_{ring} deformation + *in plane* CH_{ring} deformation + *in plane* CH bending); 1229s (Npx νC-O, *in plane* CC_{ring} + CH_{ring} deformation + *in plane* CH bending); 1195m, 1179m, 1160m (Npx νC-O + νC-C + *in plane* CH bending + δCH_3); 1028s (Npx νC-O + CH_3 rocking and cym CH_3 rocking + CH bending); 898m (cym *out of plane* CH_{ring} bending). **UV/VIS**, λ_{max} (nm) / ε ($mol^{-1}Lcm^{-1}$): 270(sh)/ n.d.; 317 / 2200; 332 / 2000; 423 / 800 (in CH_2Cl_2).

2.3 General Instrumentation and Analysis

Elemental analyses (C,H,N, Perkin-Elmer 2400 Elemental Analyzer; Cl, volumetric analysis), ESI-MS (Bruker Daltonics Micro TOF equipment, capillary, 4.5 kV, nebulizer 0.4 bar, dry gas 4.0 L min^{-1}, 200 °C, samples dissolved in chloroform/further diluted in acetonitrile), and ^{1}H NMR, ^{13}C NMR, HSQC (Heteronuclear Multiple Quantum Correlation), HMBC (Heteronuclear Multiple Bond Correlation) experiments (INOVA 300 MHz or Bruker AIII 500 MHz spectrometer, at probe temperature) were performed at the Analytical Center of the Institute of Chemistry, University of São Paulo. The electronic absorption spectra (compound solution in 1.0 cm quartz cuvettes) were recorded on a Shimadzu UV-1650 PC and the ATR/FT-IR spectra (solid samples) in a Bruker/alpha FT-IR spectrophotometer.

2.4 Fluorescence studies

The fluorescence measurements were performed in a PC1 photon-counting spectrofluorimeter (ISS) with a photomultiplier-based photon counting detector, using all-polished-side 1.0 cm quartz cuvettes. The fluorescence emission and excitation spectra of compounds (2.0 x 10^{-6} mol L^{-1} in CH_2Cl_2) were registered at room temperature (about 25^{o}C). The excitation wavelength was set at 275 nm. Relative fluorescence quantum yields (Φ_f) were determined by the equation:

$$\Phi_f = \Phi_{fs} \frac{F_u}{F_s} \frac{A_s}{A_u} \frac{n_u^{\,2}}{n_s^{\,2}}$$

where Φ_f is the fluorescence quantum yield, A is the absorbance at the excitation wavelength, F is the area under the corrected emission curve, and n is the refractive index of the solvent. Subscripts s and x refer to the standard and to the unknown, respectively [67]. Both sample and standard were excited at the same wavelength and slit condition. The absorbance of solutions at the excitation wavelength ranged from 0.01 to 0.03 to avoid the inner filter effect [67]. HNpx was used a reference standard at 2.0 x 10^{-6} mol L^{-1} in CH_3OH solution (Φ_F = 0.53) [68].

2.5 Computational methodology

The electronic calculations were performed using the GAUSSIAN 09 program [69]. Stationary points on the potential energy surface were fully optimized, followed by evaluations of the harmonic vibration frequencies to characterize their natural minima. The absence of imaginary frequencies indicated that all optimized structures were true minima. The PBE1PBE function [70,71] was used in the optimization procedure employing the

LANL2TZ basis set for the ruthenium atom [72] and 6-31G(d,p) ones for the other elements [73,74]. Nevertheless, additional DFT methods were also applied for particular purposes along this investigation as M05 [75], M05-2X [76], M06L [77], M06 [78], M06-2X [78], BMK [79], B3LYP [80,81], B97D [82], BP86 [83] and wB97XD [84]. The solvation effect was examined by the Polarizable Continuum Model (PCM) with the integral equation formalism variant (IEF-PCM) [85]. In the calculation of the bond order indice, Mayer [86], Wiberg [87] and NLMO/NPA [88] methods were applied. The Natural Population Analysis (NPA) [89] was used for the condensed dual descriptor. Natural bond orbital (NBO) analysis was carried out using the NBO 6.0 program [90]. Time-dependent Density Functional Theory [91-93] making use of the PBE1PBE functional was applied to simulate UV/VIS spectra.

2.6 Biological Assays

2.6.1 Cell culture

NCI-H460 and A549 cell lines were obtained from American Type Culture Collection (VA, USA) and Rio de Janeiro Cell Bank (RJ, BRA), respectively. Both cell lines were cultured in RPMI-1640 medium supplemented with 10% (v/v) fetal bovine serum (BSA), penicillin (100 units mL^{-1}), streptomycin (100 μg mL^{-1}) and 0.5% (w/v) amphotericin B. All cells were cultured at 37 °C and 5% CO_2 and cultures were amplified and cryopreserved in 10% dmso in BSA at - 80 °C.

2.6.2 Preparation of compound solutions

Stock solutions of compounds were prepared at 20 mmol L^{-1} in dmso and stored at -20 °C. Then, for each assay, these solutions were diluted in the culture medium having 10% FBS and 1% antibiotic/antimycotic to give final concentrations varying from 6.5 to 400 μmol L^{-1}.

2.6.3 Cytotoxicity assay

Cells were plated at the density of 10^4 cells/well in 96-well plates and, after adhesion they were treated separately with each compound at concentrations varying from 6.5 to 400 μmol L^{-1} for 24 h. Then, 10 μL of MTT ([3(4,5-dimethylthiazol-2-yl)-2,5-diphenyltetrazolium bromide], Sigma-Aldrich, MO, USA) was added to each well at 5 mg mL^{-1} and the plates were incubated for 3 h. After centrifugation at 240 g, for 10 min, the medium was removed and the formed crystals were solubilized in 100 μL dmso. Cell viability was calculated from the optical densities at 538 nm in the VERSAmax Tunable Microplate Reader, (Molecular Devices, CA, USA). The absorbance values from the control wells (exposed only to the medium with the vehicle) were used to calculate the total cell viability (100%). The

cytotoxicity is expressed by the IC_{50} (i.e., 50% inhibitory concentration of cell proliferation) values estimated from the dose-response curve of each compound.

2.6.4 Evaluation of mitochondrial membrane potential

NCI-H460 cells (2.5 x 10^5 cells / well) were treated individually with **L1** (75 and 150 μmol L^{-1}), compound **1** (75 and 150 μmol L^{-1}) and compound **3** (37.5 and 75 μmol L^{-1}) for 24 h to evaluate mitochondrial membrane potential (MMP, $\Delta\psi m$). CCCP (m-chlorophenylhydrazone carbonylcyanide, Sigma-Aldrich, MO, USA), a potent decoupler of mitochondrial oxidative phosphorylation, was used at 100 μmol L^{-1} as a positive control of mitochondrial depolarization. After treatment, cells were harvested, washed with PBS/0.5% BSA 0.5% azide and incubated for 15 min at 37°C with 50 nmol L^{-1} TMRE (ethyl ester tetramethylrodamine, Molecular Probes, OR, USA). The cells were washed again, re-suspended in 300 μL of PBS/BSA solution and analyzed on the FACSCalibur flow cytometer (Becton Dickinson, CA, USA). A total of 20,000 events were collected per sample and analyzed using the FlowJo software version 0.7 (Tree Star Inc., OR, USA).

2.6.5 Cell cycle analysis

NCI-H460 cells (2.5 x 10^5 cells / well) previously synchronized by serum starvation were treated for 24 h with compound **1** or **L1** (at 75 and 150 μmol L^{-1}), removed from the plate and washed twice with PBS / BSA 0.5% azide 0.2%. Cells were centrifuged for 10 min at 290 g, fixed and permeabilized with 70% alcohol, and after that they were kept overnight in a freezer. Finally, the cells were labeled with 0.1 mg mL^{-1} propidium iodide solution and 0.25 mg mL^{-1} RNAse. Cell fluorescence was measured on a FACSCalibur flow cytometer (Becton Dickinson, CA, USA) with CellQuest software and 10,000 events were acquired for each sample. Further analyzes were performed by using the FlowJo software version 0.7 (Tree Star Inc., OR, USA).

2.6.6 Western blotting

NCI-H460 cells treated for 24 h with compound **1** or **L1** (at 75 and 150 μmol L^{-1}) were lysed with mammalian protein extraction reagent (Mammalian Protein Extraction Reagent®, Thermo Scientific Pierce, IL, USA) containing 10% protease inhibitor and phosphatase inhibitor. Each lysate protein concentration was determined by Bradford assay. According to the obtained concentration of proteins, cell lysates were diluted in Standard Western blotting buffer (50 mmol L^{-1} Tris-HCl, pH 6.8, 2% SDS, 10% glycerol, 5% 2-β-mercaptoethanol, 0.002% blue bromophenol) and denatured by heating. Thereafter, cell lysates were fractionated by electrophoresis (SDS/PAGE, Biorad, CA, USA) and transferred to

polyvinylidene fluoride membranes. Then, the membranes were washed in Tris-saline buffer (TTBS: 100 mmol L^{-1} Tris-HCl, 137 mmol L^{-1} NaCl and 0.05% Tween-20, pH 7.8) and blocked for 1 h in 5% diluted in TTBS. After washing with TTBS, the membrane was incubated overnight with the primary antibodies anti-capase 8, capase 3, caspase 9, cytochrome c, β-actin, BAX, BAD, Bcl-Xl, Bcl-2, CDK4, CDK6, cyclin A, cyclin D1, cyclin D3, cyclin E2, NF-Ƙb, p-p53, p38, p-cdc2 at 8 °C. The membrane was washed again with TTBS and then incubated for 1 h with secondary antibody anti-mouse or rabbit conjugated to horseradish peroxidase. Detection was performed with the Pierce® Western Blotting Substrate Plus kit (Thermo Scientific Pierce, IL, USA).

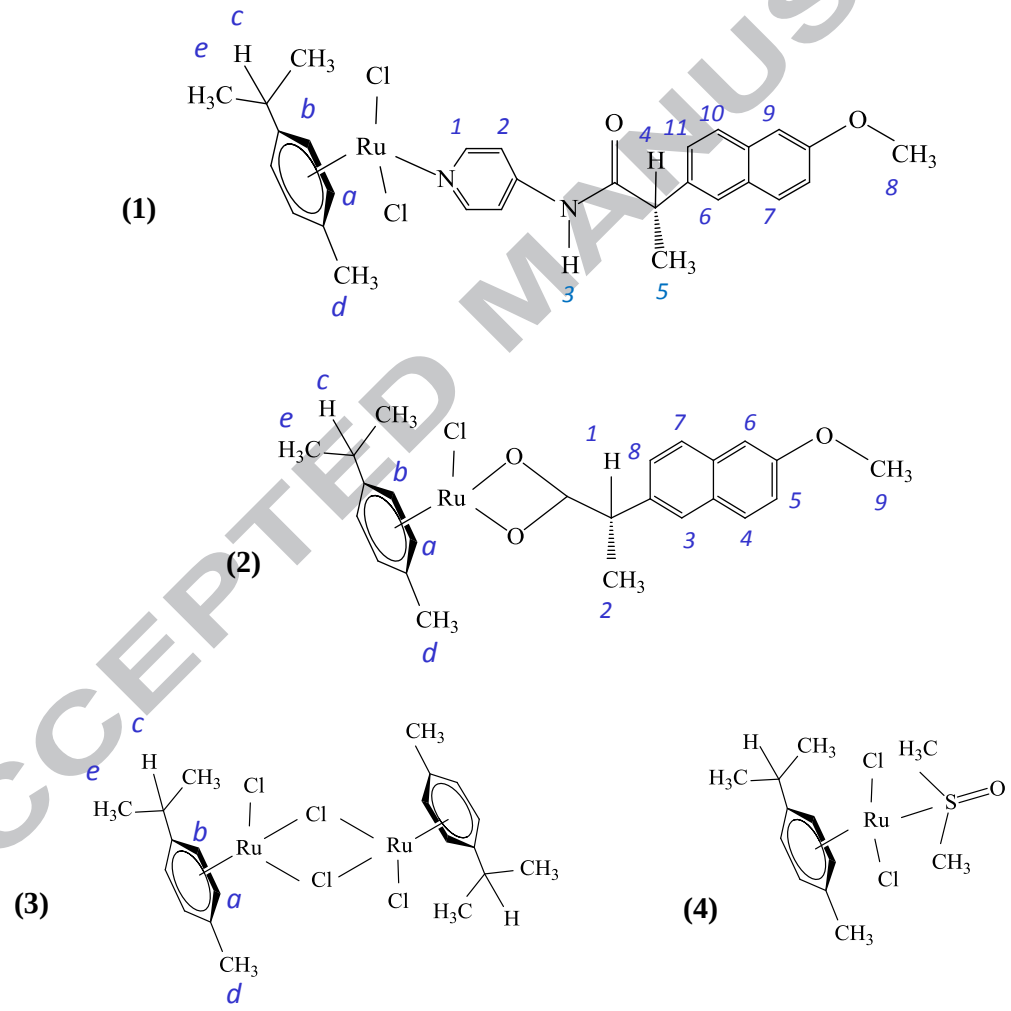

Figure 1. Structures of Ru(II)-arene compounds **1**, **2**, **3** and **4** (showing labels of hydrogens used in the ^{1}H NMR spectra assignment).

3 Results and discussion

3.1 Synthesis and characterization

3.1.1 [Ru(η^6-*p*-cymene)(L2)Cl]

The synthesis of the organometallic **2** has been improved by using only methanol, instead of the CH_2Cl_2/MeOH mixture, to achieve high yield (85 %) in much shorter time (1 h) than the overnight period needed before [64]. Single crystal structure data for this compound (not shown) were in agreement with the reported results [64], thus supporting the typical piano-stool geometry of the Ru(II)-arene bearing one chloride and bidentate naproxenate. However, the use of other techniques is crucial for reliable characterization since the crystal structure of one single crystal is not guarantee for the purity of any bulk solid. Regarding this part, disagreement in values and/or assignments, in relation to the published data, were found. The ESI-MS(+) peaks having the isotopic pattern of Ru are found here at m/z: 465.10, assigned to [Ru(cym)(**L2**)]$^+$, as previously [64]; 270.98, assigned to a fragment lacking the Npx, [Ru(cym)Cl]$^+$, not reported before; and 312.01, ascribed to [Ru(cym)(CH_3CN)Cl]$^+$, which seems more reasonable than the reported [Ru(cym)Cl(H_2O)Na] fragment [64], since if this late one is 1+ charged, it would have slightly distinct m/z (311.75) and it would be also incoherent with the Ru(II) oxidation state of the organometallic **2**.

The NMR analysis also shows discrepancies when compared with the reported data. The assignment of the ^{1}H NMR spectrum of **2** ($CDCl_3$, Appx. SM.4, Fig. S5a) is supported here by the ^{13}CNMR (Appx. SM.4, Fig. S5b) and HSQC, HMBC spectra (Appx. SM.4, Fig. S6, TS2), and it is also corroborated by the comparison with spectra of **3** ($CDCl_3$), **HL2** ($CDCl_3$ or *d*-MeOH) and **NaL2** (*d*-MeOH). Typical signals of the *p*-cymene ring hydrogens in **2** are significantly shifted upon coordination of **L2**. The shift towards downfield of the cym ring peaks (CH*b*, 5.54; CH*a*, 5.32 ppm) in relation to precursor **3** (5.48; 5.35 ppm, respectively) support the environment changes around the metal. The coordination of **L2** is corroborated by the chemical shift of the signals of the hydrogens nearly adjacent to the -COO group. Both the upfield shift of the signal of the hydrogen directly bonded to the drug chiral carbon (Npx CH_{chiral} *1*) in **2** (3.52 ppm) in relation to **HL2** (3.86, $CDCl_3$; 3.82 ppm, *d*-MeOH), and the lower value of δ when compared with the peak shifting of drug salt (**NaL2**, 3.71 ppm), for which electrostatic interactions exist, support the assignment. Taking into account this interpretation together with the expected deprotonation of naproxen upon coordination in **2**, and also the expected hydrogen shielding upon drug coordination to Ru(II), the previous assignment of the peak at 3.84 ppm [s, 4H] to Npx CH_{chiral} hydrogen/CH_3 hydrogens of CH_3(CH)COOH is questionable [64]. The hydrogen signal of Npx O-CH_3 *9* is assigned here

to the singlet at 3.92 ppm in **2**, based on the lack of significant shift when compared to the parent drug (**HL2**: 3.91, $CDCl_3$; 3.88, *d*-MeOH; **NaL2**: 3.87 ppm). The signals of the methyl group hydrogens bonded to the chiral carbon (Npx C_{chiral}-CH_3 *2*) in **2** (1.43 ppm) are assigned to a doublet (3H) shifted to higher field in relation to free drug (**HL2**: 1.58, $CDCl_3$; 1.50, *d*-MeOH; **NaL2** 1.49 ppm).

The major ATR-IR bands of **2** (experimental part) are tentatively assigned here by comparison with the spectra of **3** (Appx. SM.1.2), *p*-cymene (not shown), **HL2** (not shown) and **NaL2** (Appx. SM.1.3). The ν(C=O) typical vibrational bands of the -COOH group [94] found at 1728, 1685 cm^{-1} in **HL2** must disappear after deprotonation of the acidic drug to give the $-COO^-$ naproxenate anion (**L2**). The ν_aCOO asymmetric and ν_sCOO symmetric stretching modes of ionic **L2** appear at 1546 and 1360 cm^{-1}, respectively, in the spectrum of the **NaL2** salt, which also shows spectral changes at the region ascribable to νC-O stretching of -COO (1200-1150 cm^{-1}) when compared to the carboxylic acid spectrum. Spectrum of **2** shows typical bands of both *p*-cymene and naproxenate ligands. The major spectral changes are found at the frequency ranges: 1510-1400 and 1270-1000 cm^{-1}. The appearance of new bands in spectrum of **2**, when compared to **HL2** and **NaL2**, suggests the assignment of the ν_aCOO and ν_sCOO vibrations of the organometallic at 1460 and 1437 cm^{-1}, respectively. Although the band at 1505 cm^{-1} in **2** might be not totally ruled out for ν_aCOO (considering the usually reported ν_a frequencies of other Ru-carboxylates [95-98]), it is worthy to note that the joint analysis of all spectra here suggests high contribution of vibrational modes of both Npx and *p*-cymene ligands (δCH_3 of both Npx and cym, and νCC_{ring} of both Npx and cym) rather than only a new individual ν_aCOO band. The free **HL2** shows band at 1505 cm^{-1} while the precursor **3** (lacking carboxylate as ligand) shows aromatic ring vibration around 1500 cm^{-1} (due to lower frequency shift in relation to the free *p*-cymene (1516 cm^{-1})). The Δν(COO) difference from 1460 and 1437 cm^{-1} supports the bidentate mode of **L2** in **2** when compared to the ionic carboxylate in **NaL2**. The previous assignment [64] of ν_aCOO at 1502-1594 cm^{-1} and ν_sCOO at 1379-1385 cm^{-1} frequency ranges for **2** and other Ru(II)-*p*-cymene-NSAID compounds seems to be not characteristic of bidentate carboxylate. The bands at 1270-1000 cm^{-1} in spectrum of **2** are assigned here to νC-O modes of carboxylate. Furthermore, the spectral changes in spectrum of **2** (1229s, 1195m, 1179m, 1160m) in relation to **NaL2** (1213s, 1163m) support the distinct modes of interaction of the -COO group with the metal atoms (bidentate coordination (Ru) and ionic (Na)). Finally, the band at 898 cm^{-1}, which shifts to higher frequency in relation to those of **3** (874) and free *p*-cymene (816 cm^{-1}), is assigned to cym *out of plane* CH_{ring} bending in **2**.

3.1.2 Npxpya

The naproxen-pyridineamide (**L1)** has been prepared here in high purity (see characterization bellow with additional ESI-MS, ^{13}CNMR data not previously reported), and also in high yield (91%), by reacting **HL2** with 4-aminopyridine in the presence of DCC, in CH_2Cl_2 at room temperature, without need of any special gas atmosphere. The present synthetic procedure is advantageous when compared with the reported method [63] which is based on the coupling reaction with thionyl chloride (moisture-sensitive chemical) in benzene (toxic) solvent, conducted under argon atmosphere, and gave only 50% yield (*S*)-Npxpya. The ESI-MS(+) supports the formation of the modified drug according to the peaks at m/z: 307.14 and 329.13 ascribable to $[\mathbf{L1}+H]^+$ and $[\mathbf{L1}+Na]^+$ (Na^+ ion coming from the matrix) respectively. The assignment of the ^{1}HNMR spectrum of **L1** (experimental section, Appx. SM.2, Fig. S1a) is supported by the ^{13}CNMR spectrum (Appx. SM.2, Fig. S1b). The peaks of the pyridine ring hydrogens (CH_{py}) are at 8.40 - 7.36 ppm, while the peaks of the naphtalene ring hydrogens (Npx CH_{ring}) appear at 7.8 - 7.1 ppm. A peak at 3.93 ppm is assigned to the methyl hydrogens belonging to the O-CH_3 group (O-CH_3 *12*). The signal of the hydrogens from the methyl groups bonded to the chiral carbon (C-$CH_{3(chiral)}$ *5*) shifts to lower field (1.66 ppm) in relation to **HL2** (1.58 ppm) in the same solvent. The ATR-FT spectrum (Appx. SM.5, Fig. S7) shows the typical bands of both Npx and pyridine ring, in addition to new bands assignable to the amide group: 1702 cm^{-1} (pya νC=O), 1589 cm^{-1} (pya N-H bending) and 1506 cm^{-1} (pya ν_{ring} and Npx δCH_3).

3.1.3 [Ru(*p*-cymene)(L1)Cl_2]

Compound **1** was obtained in good yield from the reaction of **L1** with precursor **3**, in CH_2Cl_2. The ESI-MS(+) peaks having isotopic pattern of Ru are at m/z: 577.12, assigned to a fragment lacking one chloride ligand, [Ru(cym)(**L1**)Cl]$^+$; 541.14, associated to [Ru(cym)**(L1)** - 1H]$^+$; and 270.98, ascribed to a fragment lacking the **L1** ligand, [Ru(cym)Cl]$^+$. The typical piano stool geometry of the new compound is corroborated by spectroscopic characterization. The ^{1}H NMR spectral analysis of **1** (Appx. SM.3, Fig. S2a) is supported by the ^{13}C NMR (Appx. SM.3, Fig. S2b), HSQC, HMBC (Appx. SM.3, Fig. S3, TS1) and NOESY spectra (Appx. SM.3, Fig. S4), and by comparison with the signals of precursor **3** (Appx. SM.3) and compound **2** (Appx. SM.4, Fig. 4). The spectral profile of **1** confirms the changes on the metal coordination sphere, in relation to precursor **3**, which are accompanied by symmetry reduction

of the *p*-cymene associated to the presence of the Npxpya drug ligand. Shifting towards higher field upon coordination of **L1** is observed for *p*-cymene CH ring hydrogens (four doublets: CH*a*, 5.01, 4.95; CH*b*, 5.36, 5.29 ppm, compared to single doublets: CH*a*, 5.35; CH*b*, 5.48 ppm in **3**) and methyl group (cym CH_3 *d*: 1.77 in **1**; 2.16 ppm in **3**). The coordination of **L1** to Ru through the nitrogen atom in **1** is supported by the upfield chemical shift of the pyridine-ring hydrogens adjacent to the nitrogen (CH_{py} *1* at 7.93-7.83 (m) coupled to Npxpya CH_{ring} *6,7,10* ; CH_{py} *2* at 6.96 (d), ppm), in relation to the free **L1** (8.40 (dd); 7.36 (dd), ppm). The signal of the isopropyl group hydrogens also shifts to higher field (in ppm: $CH(CH_3)_2$(c) 2.81 (m), 1H; $CH(CH_3)_2$(e) 1.24 (m), 6H) in comparison with the signals of **3** (2.92 (m), 1H; 1.28 (d), 6H, respectively). The ^{13}C NMR spectrum of **1** shows chemical shifts of carbons belonging to the pyridine ring towards downfield upon coordination of **L1**: N_{py}-***C***H (from 150.48 in **L1** to 154.13 ppm in **1**), HN-C_{py} (145.03 to 146.42) and CH_{py} (113.41 to 115.01 ppm) which corroborate the coordination of the *N*-pyridine to ruthenium.

The presence of the Npxpya in **1** is corroborated by the ATR-IR spectrum (Appx. SM.5, Fig. S7). Compound **1** shows the three typical major bands assignable to **L1** (ν(cm^{-1}): 1702, pya νC=O; 1590s, pya N-H bending; 1502vs, pya νCN_{ring} + νCC_{ring} and Npx δCH_3); 1424m, pya ν_{ring}). The band of pyridine ring breath (1417 cm^{-1} in **L1**) slightly shifts to higher frequency (1423 cm^{-1} in **1**), thus confirming the coordination of **L1** to Ru through the *N*-pyridine atom. Other relevant spectral changes occur at the regions 1230-1100 cm^{-1} (νCC_{ring}), 1100-1000 cm^{-1} (ring breathing) and 900-700 cm^{-1} (out of plane CH py ring). The bands of *p*-cymene were difficult to assign due to overlap with bands of **L1** at 1500-1300 cm^{-1}, although spectral changes could be observed in relation to precursor **3**.

3.2 Computational analysis of structures

Computational structural analysis was performed for both Ru(II)-arenes and Npxpya (Appx. SM.6). The DFT analysis of **2** by PBE1PBE is in good agreement with the crystal structure reported data [64] (Appx. SM. 6, Fig. S8; SM.6.1, TS3). Good structural description was also obtained by B3LYP, B97D, BP86, M05, M06, M06L, wB97XD methods, although these outperformed Ru-Cl and Ru-O bond lengths compared to PBE1PBE (Appx. SM.6.1, TS3, TS4). DFT bond order data suggests a Ru metal center dominated by σ-bonds with NLMO/NPA bond indices: Ru-C, 0.45-0.47; Ru-Cl, 0.52; Ru-O, 0.19-0.25 (Appx. SM.6.1, TS5). The C-O bond shows partial double character (between σ and π) corroborating the bidentate coordination of the **L2** drug ligand. Compound **2** shows C-O NPA charge separation higher than MeOH and slightly lower than CO_2 molecule (Appx. SM.6.1, TS6). The DFT

structural analysis of the new organometallic **1**, due to the lack of crystallographic data, was based on the DFT most stable calculated structure for **L1** (predominant conformer at 52%, see discussion Appx. SM.6.2, Fig. S9; TS7, TS8), and has been performed by using different DFT methods (Appx. SM.6.3, TS9). The relative Gibbs free energy of six possible structures predicted for **1** by PBE1PBE in CH_2Cl_2 IEF-PCM solvent pointed to the most stable structure at 63% contribution (Appx. SM.6.3, Fig. S10). Taking into account all the methods used here (Appx. SM.6.1, TS3; SM.6.3, TS9; SM.6.4, TS11) for both Ru(II)-arenes, the bond lengths are at the ranges 2.400-2.445 Å (Ru-Cl) and 2.135-2.217 Å (Ru-N). The Ru-C bond distances are slightly longer in **1** (2.154-2.300 Å) than in **2** (2.138-2.259 Å). The coordination sphere of **1**, represented by σ–bonds, shows low bond order reflecting small covalent character for the Ru–N bond (Appx. SM.6.3, TS10) [99]. The molecular electrostatic potential maps (Appx. SM.6.4, Fig.S11) suggest similar distribution of electron density with the negative regions mainly located on the naproxen moiety for both Ru(II)-arenes, while extensive positive regions are predicted along the coordination sphere, and particularly extended to the pyridine ring in the case of **1**.

3.3 Chemical behavior of the Ru(II)-arenes in dmso

Studies about the stability of compounds bearing the moiety [Ru(η^6-*p*-cymene)(L)] with different types of ligands, as for example, monodentate or bidentate ligands having *N*- [100], *P*- [101, 102] or *O*- [103-105] donor atoms, indicate dissociation of the L-ligand, and/or also of the arene, when the organometallic is dissolved in dmso or water (solvents commonly used to prepare solutions of drugs in biological assays). Taking into account that both of the Ru(II)-arenes investigated here were dissolved in dmso for the biological experiments, we have monitored their chemical behavior by following the ^{1}H NMR spectral changes in *d*-dmso as a function of the time compared to the spectra of the precursors and parent ligands (Appx. SM.7).

The ^{1}H NMR spectra of both **1** and **2** compounds show significant changes in relation to their spectra in $CDCl_3$, suggesting that, differently from the behavior in the non-coordinating chloroform, they are not stable in dmso. In the case of **2**, the spectral changes (Appx. SM.7, Fig.S12) suggest transformations that start shortly after the dissolution, in disagreement with the previous report [64] which claims that this compound is stable up to 12 h. The peaks of Npx CH_{ring} (CH_{ring} *3,4,7* at 7.9-7.6; CH_{ring} *8* at 7.5-7.3; CH_{ring} *5,6* at 7.3-7.0 ppm) which appear nearest to the signals of **NaL2** at the beginning, decrease in intensity in the subsequent times, while new peaks closest to the signals of **HL2** arise. Similar behaviour

occurs at the region of Npx C_{chiral}-CH_3 *9*, what may suggest possible transformation of species having bidentate- to species bearing monodentate- Npx drug ligand. Subsequent and gradual spectral changes over the time indicate predominant dissociation of the drug ligand accompanied by the formation of the substituted Ru(cym)dmso species **4** (5.82 (d), CH*b*; 5.77, CH*a*; 2.82 (m), CH*c*-$(CH_3)_2$, 1.16 (d) ppm, CH$(CH_3e)_2$). The findings indicate that **2** readily undergoes chemical transformations, apparently involving changes on the coordination mode of **L2**, that are followed by the dissociation of the drug ligand. The process may involve equilibrium among distinct species that seems to be not finished after 48 h (the maximum time investigated here). The literature proposal for protonation of **L2** to **HL2**, based on a peak at 9.7 ppm [64] might be unlike to happen since the typical peak of free **HL2** in *d*-dmso is observed here at 12.3 ppm. We have also observed low intensity peaks at 9.7 and 9.8 ppm after 24 h, but although these appear are located at the downfield typical region of hydrogen-bonded species, they could not be undoubtable assigned.

In contrast to **2**, the new organometallic **1** was found to lose its integrity by prompt total dissociation of the **L1** ligand. The ^{1}H NMR spectrum (Appx. SM.7, Fig.S13) registered shortly after dissolution of **1** in *d*-dmso gives evidence for the lack of the original organometallic while it confirms the presence of the substituted Ru(cym)dmso species **4** (CH*a*, 5.82 (d); CH*b*, 5.78 (d); CH_3d, 2.08 ppm) and the **L1** free drug [peaks of the pyridine-ring hydrogens adjacent to the *N* atom (in $CDCl_3$, at 7.93-7.83 (m), CH_{py} *1*, coupled to CH_{ring}; and at 6.96 (d) ppm, CH_{py} *2*) shift towards downfield reaching resemblance to the free **L1** (in dmso, 8.40 (d); 7.82-7.12 ppm (m); amide group N-H hydrogen, around 10.5 ppm].

It is worthy to highlight that the time-dependent spectra of the Ru(II)-arenes were compared with the spectrum of the free *p*-cymene (in *d*-dmso, peaks at: 7.12-7.05; 2.89-2.75; 2.25; 1.18,1.16 ppm) to check for possible dissociation of the *p*-cymene ring, since this has been recently reported for other Ru-(*p*-cymene) bearing NSAID-carboxylates [105]). In the case of compound **2**, bearing the bidentate naproxenate, no evidence is found for appreciable dissociation of the *p*-cymene ring. Furthermore, in the case of **1**, bearing the *N*-coordinated Npxpya, the spectrum clearly indicates the presence of only two species, *i.e.*, Npxpya (**L1**) and Ru(cym)dmso species (**4**), shortly after its dissolution in dmso.

3.4 Electronic absorption spectra

The electronic absorption properties of both Ru(II)-arenes are described here for the first time. Experimental λ_{max}, DFT PBE1PBE computed wavelengths and the assignment of electronic transitions based on electron density of the frontier molecular orbitals (Appx. SM.8,

Fig. S14, TS12) are presented in Table 1. Compound **2** shows intense bands at 270 (sh), 317 and 332 nm, and a relatively less intense band centered at λ_{max} 423 nm. Similar UV bands are found for **HL2** (λ (nm) /ε ($mol^{-1}Lcm^{-1}$): 230/n.d.; 260/4400; 270/4500; 317/1300; 330/1500, in methanol) and an intense band at 270 nm is also observed for precursor **3** (Appx. SM.1.3). The DFT PBE1PBE calculations suggest contributions of metal-to-ligand charge transfer (MLCT) and intraligand (LL) transitions at 260-290 nm. The bands at 317, 332 nm are predicted mainly as LL transitions, although a band at 340 nm is also observed for **3**. The visible band (423 nm) is assigned predominantly as MLCT transition. The shift of this band when precursor **3** is dissolved in different solvents (450 nm in CH_2Cl_2; 418 nm in CH_3CN; 400 nm in dmso, spectra not shown) may corroborate the contribution of the Ru-*p*-cymene framework as the "metal part" in the MLCT transition. A visible band at the same region has been assigned to metal-to-ligand transition for other ruthenium organometallics [106-108]. Compound **1** exhibits electronic spectrum dominated by high intensity UV shoulders which extends up to the beginning of the visible region, what makes the interpretation of the electronic absorptions more complicated. Intense shoulders at 275-285 nm and a relatively less intense shoulder at 332 nm, in addition to a visible band around 406 nm, are observed. The UV absorptions are similar to those found for **L1** (λ (nm) /ε ($mol^{-1}L\ cm^{-1}$): 275(sh)/n.d.; 285(sh)/5000; 318/1800; 333/2000, in CH_2Cl_2). However, computational analysis predicts contributions of both MLCT and LL transitions for the UV bands of **1**. The band at 406 nm is overlapped with part of the UV absorptions, what might explain the participation of LL transitions also at the visible. Despite the band overlap, it is interesting to note that the visible band of **1** shifts to higher energy (lower λ, 406 nm) when compared with **2** (423 nm) and **3** (450 nm) in the non-coordinating dichloromethane.

Regarding the analysis of electron density of the frontier molecular orbitals (Appx. SM.8, Fig. S14, TS12), it is interesting to mention that the energy gap between the highest occupied molecular orbital (HOMO) and the lowest unoccupied molecular orbital (LUMO) is similar for both Ru(II)-arenes (~4.2 eV) suggesting similar kinetic stability [109]. While the π^* LUMO orbitals are distributed in the naproxen moiety in **2**, the π^* LUMO orbitals of **1** are predominantly distributed in the pyridine ring having small participation in the amide group. The data show that the Ru *d*-orbitals contribute mainly in the H-2 and L+4 molecular orbitals, in good accordance with other studies [110,111]. The Ru t_{2g} orbitals contribute mainly in H-1 and H-2, whereas the antibonding d_{z^2} orbital shows minor contribution in L+1 and L+4 molecular orbitals of **2** and **1**, respectively. Notwithstanding an antibonding combination from oxygen lone pair electrons of the carboxylate moiety is seen in the L+1 molecular orbital of **2**,

the combination comes delocalized from the antibonding naproxen π part and from oxygen lone pair electrons in the ligand in the case of the L+4 molecular orbital of compound **1**

Table 1. Major bands (λ_{max}) at the experimental electronic absorption spectra of Ru(II)-arenes in dichloromethane and computed DFT PBE1PBE calculated wavelenghts (λ_{calc}).

Compound	**λ_{max} (nm) / ε ($mol^{-1}Lcm^{-1}$)***	**λ_{calc} (nm)**	**Transition****
1	280	291.3	LL
		302.0	MLCT
	332 / 4000	317.3	LL
		351.2	MLCT
	406 / 800	407.5	LL
		418.4	MLCT / LL
		482.5	LL
2	270	265.5	MLCT / LL
		281.5	MLCT
	317 / 2200	318.5	LL
	332 / 2000	328.2	LL
	423 / 800	449.7	MLCT

* The values of molar absorptivity were estimated directly from the absorbance in the spectrum without deconvolution. ** Assignment: LL = intraligand electronic transition; MLCT = metal to ligand charge transfer electronic transition.

3.5 Fluorescence studies

The photophysical properties of the Ru(II)-arene compounds are reported here also for the first time. Both organometallics **1** and **2** show fluorescence spectra similar to those of their correspondent parent ligands. The emission band assignable to the naphthalene fluorophore [60] is found at 350 nm (Appx. SM.9, Fig. S15). The large Stokes shift values (Table 2) might be related to significant structural changes on the ground and the excited states upon photo-excitation. The lack of self-absorption which may facilitate the distinction between emission and excitation suggests attractive photophysical property [112]. Similar behavior is observed in Re(I) [112] and other Ru(II) [113] compounds. **L1** shows emission quantum yield (Φ_f = 0.25, CH_2Cl_2) lower than those found for the **HL2** drug (0.40, aqueous buffer [60]; 0.47, CH_3CN [114]; 0.53, CH_3OH [67]). The decrease in the Φ_f of the Ru(II)-arenes (0.04 (**1**); 0.22 (**2**), Table 2), in relation to those of their corresponding parent ligands, might be explained by the metal coordination to the fluorophore ligand inducing fluorescence quenching [115,116,117]. Moreover, the pyridineamide moiety in **1** may act as a bridge in the metal-naproxen donor-acceptor conjugate system promoting additional fluorescence quenching, in consistency with other reported data [118-120].

Table 2. Photophysical data of Ru(II)-arene compounds

Compound	λ_{max} (nm)		Stokes*	Φ_f
	Excitation	Emission		
L1 (in CH_2Cl_2)	260	356	96	0.25
1 (in CH_2Cl_2)	266	356	90	0.04
L2 (in MeOH)	230, 260 sh, 270	354	84	0.53 [67]
2 (in CH_2Cl_2)	236, 274	356	82	0.22

* Determined from the difference between the maximum wavelengths of the excitation and the emission bands; sh = shoulder.

These findings also may drive future studies based on fluorescence quenching to investigate interactions of biomolecules, such as DNA and albumin, with naproxen-containing metal compounds. Compound **2** exhibits intense emission band at about 350 nm, assignable to the presence of the naproxen drug, which may overlap with the emission bands of biomolecules. Therefore, the interference from naproxen emission could only be avoided by appropriate choice of the emission wavelength in studies with biomolecules [121]. Both Ru(II)-arenes also show absorption at the UV spectral region what would require correction for inner-filter effect [122]. None of these problems have been mentioned in the previous report describing the interaction of **2** with biomolecules [64].

3.6 Biological Studies

3.6.1 Anti-proliferative effects on lung cancer cell lines

The two Ru(II)-arene compounds and their correspondent parent drugs were screened *in vitro* against two different ling cancer cell lines, A549 and NCI-H460, to evaluate the cytotoxicity (in terms of IC_{50}, the concentration of the drug that causes 50% inhibition in cell viability). No significant anti-proliferative activity was found for compound **2** and the **NaL2** drug salt, after 24 h treatment, in both cell types (IC_{50} > 200 μmol L^{-1}, Table 3). These findings are in disagreement with the previous report [64] which claims a marked antiproliferative activity (nanomolar concentration) for **2** against A549 lung cancer cells. The reason for the discrepancy between these results is difficult to establish. Firstly, compound **2** is unstable in dmso since gradual dissociation of the **L2** ligand leads to distinct species which may coexist in equilibrium, and hence the composition of species in the biological medium may be different depending on the bioassay experimental conditions. More importantly, we have conducted the assay by the MTT method [123], while the literature data [64] are based

on the Sulforhodamine B assay (SRB) [124]. MTT method relies on measuring metabolic activity to investigate the anticancer efficacy expressed by the values of IC_{50}, whereas the SRB method is based on the property of SRB to bind proteins under mild acidic conditions and the cytotoxicity results are expressed in terms GI_{50} (concentration of the drug that produces 50 % inhibition of the cells). Although both methods can be used for *in vitro* anticancer drug screening, each one shows its own peculiarities and chemosensitivity, which depend on the type of cell line. The differences in data from these two methods, however, should not be highly significant [125,126], and, moreover, cytotoxicity data from distinct methodologies, by considering all variables, should not exhibit difference much higher than 20%, in general. Therefore, the difference between our results (IC_{50} > 200 μmol L^{-1}) and the reported data (GI_{50} at nanomolar) [64] should not be so high as it is found to be for compound **2**. Another relevant aspect to be taken into account is the fact that since the SRB dye stains the total protein content in the cell, the SRB assay may not discriminate the cells that have changed their metabolic activity after the treatment but retained the protein content [127]. Furthermore, the arresting of the cells in the S phase of the cell cycle might be wrongly interpreted as a cell death effect.

The modified drug **L1** shows antiproliferative effects in both A549 and NCI-H460 lung cancer cells (IC_{50} = 158.8 and 136.10 μmol L^{-1}, respectively), despite exhibiting IC_{50} higher than the paclitaxel anticancer positive control (46.49 and 30.53 μmol L^{-1}, respectively). The anticancer activity of **L1**, contrasted to the inactivity of naproxen (Table 3), reveals that the structural modification, by inserting the amide moiety into the structure of naproxen, to give the pyridineamide-naproxen conjugated drug, is crucial for the anticancer activity. The treatment with the new organometallic **1** also led to the inhibition of cell proliferation against both lung cancer cell lines (IC_{50}: 161.00 and 145.30 μmol L^{-1}, for A549 and NCI-H460 respectively), thus giving support to the key role of **L1** to decrease cell viability. It is worth to mention that although the IC_{50} values of **1** are slightly higher than those found for the **L1** free drug, the differences between them are small (Table 3). These findings, at the time biological assays were performed, raised the suspicion that organometallic **1** might undergo ligand dissociation in dmso (phenomenon that was further confirmed by the time-dependent ^{1}H NMR studies discussed above), being that the antiproliferative activity could be due only to the free **L1**. However, further experiments on the effects on mitochondrial membrane potential (discussed below) suggest that Ru-species may play key role in mechanisms associated to drug activity when cells are treated with compound **1**.

Table 3. *In vitro* cell viability against A549 and NCI-H460 lung cancer cells.

Compound	IC_{50} values ± SD (μmol L^{-1})	
	A549	NCI-H460
1	161.00 ± 12.09	145.30 ± 13.23
L1	158.80 ± 4.47	136.10 ± 9.02
2	> 200	> 200
NaL2	> 200	> 200
Paclitaxel	46.49 ± 13.07	30.53 ± 7.21

Data presented as mean ± standard deviation of three independent experiments.
IC_{50} = half maximal inhibitory concentration. SD = standard deviation.

3.6.2 Effects on Mitochondrial Membrane Potential

The Npxpya drug (**L1**) and organometallic **1** were investigated for possible mechanisms associated to drug activity in the NCI-H460 cell line. The mitochondrial membrane potential (MMP) is a key parameter for investigating mitochondrial function since the MTT assay is based mainly in mitochondrial metabolic activity and this organelle plays crucial role in cell death pathways. CCCP and paclitaxel were used as positive controls for mitochondrial membrane depolarization and apoptosis process, respectively. The effects of the drugs (**1** and **L1**) were evaluated in two different drug concentrations (75 and 150 μmol L^{-1}). Experiments were also performed for precursor **3** (37.5 and 75 μmol L^{-1} which gives 75 and 100 μmol L^{-1} of dmso-species **4**, respectively). The results show that the MMP is significantly decreased ($p < 0.001$) in the presence of the **L1** free drug, at a concentration (150 μmol L^{-1}) close to the drug IC_{50} (Figure 2). The finding indicates that the mechanism related to the Npxpya drug activity might be mainly associated to anti-proliferative effects. Conversely, no significant effects on the MMP (Figure 2) are found when the cells are treated with compound **1** or precursor **3** (which generates Ru(cym)-dmso species **4** in dmso). Since we know at this point that organometallic **1** undergoes complete dissociation in dmso to give species **4** and **L1**, it is reasonable to think that the presence of Npxpya-free Ru species, probably in the form of species **4**, might play a role in inhibiting the mechanism related to the mitochondrial function when cells are treated with **1**, in comparison with the cell treatment with the **L1** free drug.

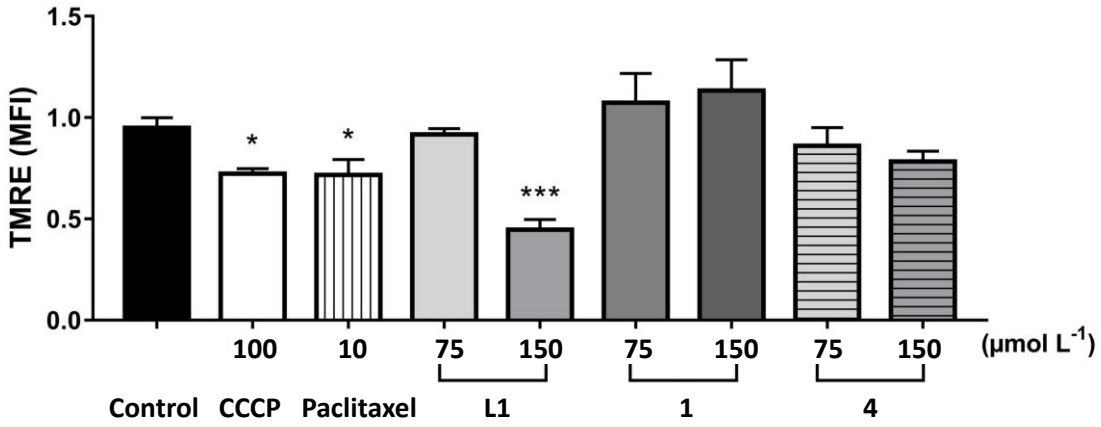

Figure 2. Flow-cytometry analysis of NCI-H460 cells, after 24 h treatment with **L1** and **1** (at 75 and150 μmol L^{-1}) and Ru(cym)-dmso species **4** (from **3** at 37.5 and 75 μmol L^{-1}), stained with TMRE. CCCP and paclitaxel were used as positive controls for mitochondrial membrane depolarization and apoptosis process, respectively. The mean fluorescence of positive cells was used to assess changes in the MMP. The data are the means ± SD from three independent experiments. * $p < 0.05$ vs. control and *** $p < 0.001$ vs. control.

3.6.3 Cell Cycle arrest

The anti-proliferative activities were evaluated by investigating the cellular distribution among the cell cycle phases by flow cytometry. Nocodazol and paclitaxel were used as positive controls of G2/M and G0/G1 arrests, respectively. Both **L1** and **1** were found to arrest cells in S-phase at concentration (75 μmol L^{-1}) lower than their IC_{50} values, and to arrest G0/G1-phase at 150 μmol L^{-1} (Figure 3a), what suggests a cytostatic mechanism of action. The findings are corroborated by Western blotting protein expression analysis by the monitoring of several proteins related to cell death (Figure 3b) and cell cycle progression (Figure 3c) (rTRAIL was used as a positive control for apoptosis). Npxpya (**L1**) shows an apoptotic feature even at 75 μmol L^{-1}, by inducing caspase 3 cleavage and reduction of anti-apoptotic proteins such as Bcl-2 and Bcl-xL (Figure 3b). By it turns, compound **1** also leads to reduction of Bcl-2 and Bcl-X Bcl-2 and Bcl-xL l, at 75 μmol L^{-1}. Nevertheless, both **L1** and **1** also promote the reduction of apoptotic proteins, such as BAD and BAX, which probably makes the scenario not favorable enough to apoptosis, leading to unchanged expression of caspase 8 and 9 cleaved and even reduction of cytochrome c. Concerning the cell cycle progression proteins (Figure 3c) **L1** and **1** are found to reduce cyclin-dependent kinase 4 and 6, cyclins A, D1, D3 and E2, which are mitogenic proteins, and also p-cdc2, which has dephosphorylation related to mitosis. In addition to the damage caused by both **L1** and **1**

leading to a reduction of p38 inactive and to an increase of p-p53 by **L1** at 150 μmol L^{-1}, the anti-apoptotic feature mentioned before is confirmed by NF-ƙB reduction.

Conclusions

The new half-sandwich organometallic **1** of formula [Ru(η^6-*p*-cymene)(**L1**)Cl_2], where **L1** is the *N*-coordinated naproxen-pyridinamide, was successfully synthesized and characterized, as well as the **L1** parent drug ligand. The reported compound **2**, [Ru(η^6-*p*-cymene)(**L2**)Cl], bearing bidentate naproxenate was re-prepared and additional investigation was performed. DFT computational calculations corroborate the proposed structures for both Ru(II)-arene compounds. The time-dependent ^{1}HNMR shows that both organometallics, despite the good stability in non-coordinating solvents, undergo dissociation in dmso to give Ru(cym)-dmso species **4** and the corresponding free drug ligand. Distinct behavior indicates that while compound **2** loses **L2** gradually, the dissociation of **L1** from compound **1** occurs instantaneously shortly after dissolution. The experimental data from electronic absorption spectroscopy shows good correlation with the DFT computational calculations. Luminescence properties of both Ru(II)-arenes, mainly associated to the naproxen moiety, suggest potential applications based on photoactivity, and may guide future studies based on fluorescence quenching to investigate interactions of compounds of this type with biomolecules. The Ru(II)-arene compounds show distinct behavior against NCI-H460 and A549 lung cancer cell lines. The treatment of the cells with **2** indicates no anticancer activity, while the treatment with the new organometallic **1** led to the inhibition of cell proliferation similarly to the **L1** free drug. These findings give evidence for the crucial role of the structural modification of naproxen (by the insertion of the amide moiety into the original structure of the drug to form the naproxen-pyridineamide conjugate) in promoting anticancer activity. The **L1** parent free drug was found to decrease significantly the mitochondrial membrane potential (MMP) in NCI-H460 cells, while compound **1**, as well as species **4** (generated from dissolution of **3** in dmso), exhibits no significant effects on the MMP. Interestingly, since ^{1}HMNR studies indicate that organometallic **1** is completely dissociated in dmso (the solvent used to prepare the drug solutions for cell treatment in the biological assays) to give the **L1** free drug and species **4**, it is plausible to infer that the presence of Npxpya-free Ru species, probably in the form of species **4**, might play a role in inhibiting the mechanism related to the mitochondrial function when cells are treated with **1**, in comparison with the cell treatment with the **L1** free drug.

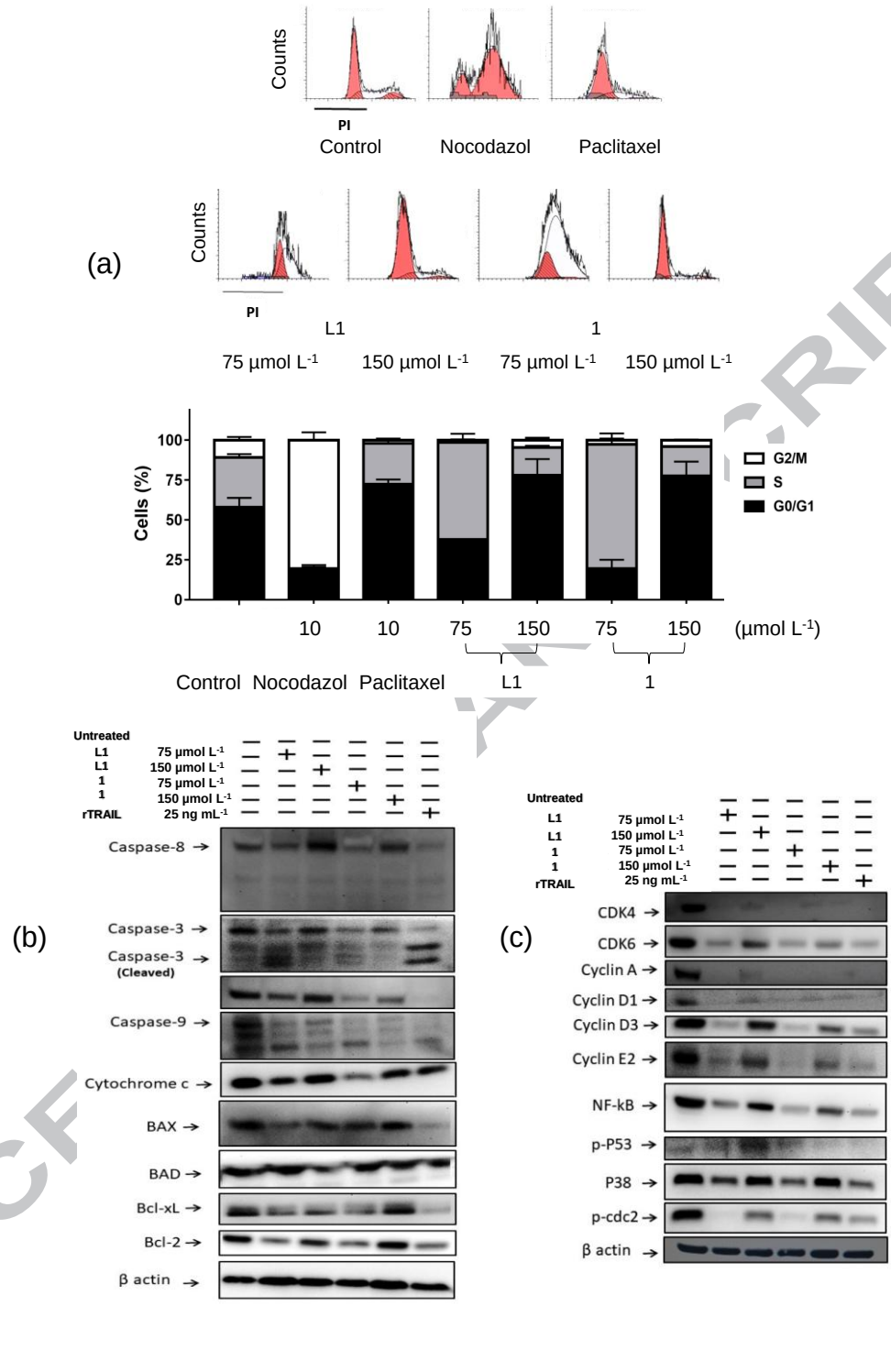

Figure 3. (a) Cell cycle phases G0/G1, S, and G2/M indicated in both the histogram and bars of % cell population distribution (data are the mean ± SD from three independent experiments); (b) Western blotting analysis of proteins expression related to cell death; (c) Cell cycle progression. rTRAIL 25 ng/mL was used as a positive control for apoptosis. β-Actin levels were used as loading control. Images are representative of at least three independent experiments.

Acknowledgements

The authors gratefully acknowledge the financial support to perform the present work to the Brazilian agencies: Fundação de Amparo à Pesquisa do Estado de São Paulo (FAPESP, research grants to D. de Oliveira Silva [2014/23047-5 and 2018/00297-4] and to A. K. Ferreira [2015/18528-7]), Conselho Nacional de Desenvolvimento Científico e Tecnológico (CNPq fellowships, for productivity to D. de Oliveira Silva [305914/2015-4] and to A. K. Ferreira [304255/2017-3], and for Master Project to S. Q. Martinez), and Coordenação de Aperfeiçoamento de Pessoal de Nível Superior (CAPES, finance code 001; Doctorate fellowships to J. P. G. Tabares, J. L. Cassiano, A. C. Stábile). The authors sincerely acknowledge Prof. P. S. Santos and J. A. A. Castilho (doctorate student) for registration of the IR spectra at Laboratory for Molecular Spectroscopy (LEM), Prof. L. Marzorati, Prof. N. Y. M. Iha and Prof. H. E. Toma for technical support, at Institute of Chemistry, University of São Paulo; Prof. L. C. Salay and L. A. Santos (bachelor student) at University of Santa Cruz. The authors are also grateful to Prof. K. P. M. Frin at Federal University of ABC (for suggestions on fluorescence studies); to the Center for Scientific Computing (NCC/GRIGUNESP) of the São Paulo State University (UNESP) and Centro Nacional de Processamento de Alto Desempenho (CENAPAD-SP) (for provision of computational facilities); and to the Alchemy, Innovation, Research & Development.

Appendix A. Supplementary material (SM.)

References

[1] M. Gielen, E.R.T. Tiekink, Eds. *Metallotherapeutic Drugs & Metal-based Diagnostic Agents - The use of metals in medicine,* 2005, John Wiley & Sons Ltd., West Sussex.

[2] E. Alessio, Ed. *Bioinorganic Medicinal Chemistry*, 2011, Wiley-VCH Verlag & Co. KGaA, Weinheim.

[3] D. de Oliveira Silva. *Ruthenium Compounds Targeting Cancer Therapy*. In Atta-ur-Rahman, M. I. Choudhary, Eds, *Frontiers in Anti-Cancer Drug Discovery*, 2014, Bentham Science Publishers Ltd**.,** Sharjah, vol. **4**, 88-156.

[4] W. H. Ang, P. J. Dyson, *Eur. J. Inorg. Chem*., 2006, **20**, 4003-4018.

[5] D. de Oliveira Silva, *Anti Canc. Agents Med. Chem.*, 2010, **10**, 312-323.

[6] M.A. Jakupec, M. Galanski, V.B. Arion, C.G. Hartinger, B.K. Keppler. *Dalton Trans*, 2008, **2**, 183-194.

[7] I. Kostova, *Curr. Med. Chem*., 2006, **13**, 1085-1107.

[8] **A.** Bergamo, G. Sava, *Dalton Trans***,** 2007, **13**, 1267-1272.

[9] A. Levina, A. Mitra, P.A. Lay, *Metallomics*, 2009, **1**, 458-470.

[10] G.S. Fink, *Dalton Trans.*, 2010, **39**, 1673-1688.

[11] W.H. Ang, A. Casini, G. Sava, P.J. Dyson, *J. Organomet. Chem*., 2011, **696**, 989-998.

[12] G. Sava, A. Bergamo, P.J. Dyson, *Dalton Trans.*, 2011, **40**, 9069-9075.

[13] G. Gasser, I. Ott, N. Metzler-Nolte, *J. Med. Chem*., 2011, **54**, 3-25.

[14] A. Bergamo, C. Gaiddon, J.H.M. Schellens, J.H. Beijnen, G. Sava, *J. Inorg. Biochem*., 2012, **106**, 90-99.

[15] C.G. Hartinger, N. Metzler-Nolte, P.J. Dyson, *Organometallics*, 2012, **31**, 5677-5685.

[16] S. Komeda, A. Casini, *Curr. Top. Med. Chem*., 2012, **12**, 219-235.

[17] G. S. Fink, *J. Organom. Chem*., 2014, **751**, 2-19.

[18] A. A. Nazarov, C. G. Hartinger, P. J. Dyson, *J. Organom. Chem.*, 2014, **751**, 251-260.

[19] M. J. Thun, S. J. Henley, C. Patrono. *J. Nat. Cancer Inst.*, 2002, **94**, 252-266.

[20] T. Tanaka, T. Kojima, N. Yoshimi, S. Sugie, H. Mori, *Carcinogenesis*, 1991, **12**, 1949-1952.

[21] P. J. Hu, J. Yu, Z. R. Zeng, W. K. Leung, H. L. Lin, B. D. Tang, A. H. Bai, J. J. Sung, *Gut*, 2004, **53**,195-200.

[22] R. E. Harris, S. Kasbari, W.B. Farrar, *Oncol. Rep*., 1999, **6**, 71-73.

[23] T. Hida, J. Leyton, A. N. Makheja, P. Ben-Av, T. Hla, A. Martinez, J.Mulshine, S. Malkani, P. Chung, T.W. Moody, *Anticancer Res.*, 1998, **18**, 775-782.

[24] J. E. Weder, C. T. Dillon, T. W. Hambley, B. J. Kennedy, P. A. Lay, J. R. Biffin, H. L. N. Regtop, M. Davies, *Coord. Chem. Rev.*, 2002, **232**, 95-126.

[25] C. N. Banti and S. K. Hadjikakou, *Eur. J. Inorg. Chem.*, 2016, 3048-3071.

[26] F. A. Cotton, D. de Oliveira Silva, *Inorg. Chim. Acta*, 1996, **249**, 57-61.

[27] A. Andrade, S.F. Namora, R.G. Woisky, G. Wiezel, R. Najjar, J.A.A. Sertié, D.de Oliveira Silva, *Inorg. Biochem.*, 2000, **81**, 23-27.

[28] C. R. Gordijo, C. A. S. Barbosa, A. M. C. Ferreira, V. R. L. Constantino, D. de Oliveira Silva, *J. Pharm. Sci.*, 2005, **94**, 1135-1148.

[29] D. J. Martins, Hanif-Ur-Rehman, S. R. Alves Rico, I. M. Costa, A. C. P. Santos, R. G. Szszudlowski, D. de Oliveira Silva, *RCS Advances*, 2015, **5**, 90184-90192.

[30] G. Ribeiro, M. Benadiba, A. Colquhoun, D. de Oliveira Silva, *Polyhedron*, 2008, **27**, 1131-1137.

[31] M. Benadiba, R.R.P. Santos, D. de Oliveira Silva, A. Colquhoun, *J. Inorg. Biochem*., 2010, **104**, 928-935.

[32] M. Benadiba, I.M. Costa, R.L.S.R. Santos, F.O. Serachi, D. de Oliveira Silva, A. Colquhoun, *J. Biol. Inorg. Chem*., 2014, **19**, 1025-1035.

[33] R.L.S.R. Santos, A. Bergamo, G. Sava, D. de Oliveira Silva, *Polyhedron*, 2012, **42**, 175-181.

[34] R.L.S.R. Santos, R.N.F. Sanches, D. de Oliveira Silva, *J. Coord. Chem*., 2015, **68**, 3209-3228.

[35] Hanif-Ur-Rehman, T.E. Freitas, R.N. Gomes, A. Colquhoun, D. de Oliveira Silva. *J. Inorg. Biochem*., 2016, **165**, 181-191.

[36] S.R. Alves Rico, A.Z. Abbasi, G.Ribeiro, T.Ahmed, X.Y. Wu, D. de Oliveira Silva. *Nanoscale*, 2017, **9**, 10701-10714.

[37] G. Sava, S. Zorzet, C. Turrin, F. Vita, M. R. Soranzo, G. Zabucchi, M. Cocchietto, A. Bergamo, S. DiGiovine, G. Pezzoni, L. Sartor, S. Garbisa, *Clin. Cancer Res*., 2003, **9**, 1898-1905.

[38] A. Bergamo, B. Gava, E. Alessio, G. Mestroni, B. Serli, M. Cocchietto, S. Zorzet, G. Sava, *Int. J. Oncol*., 2002, **21**, 1331-1338.

[39] C.G. Hartinger, S.Z-Seifred, M.A. Jakupec, B. Kynast, H. Zorbas, B. Keppler, *J. Inorg. Biochem*., 2006, **100**, 891-904.

[40] B. Schoenhacker-Alte, T. Mohr, C. Pirker, K. Kryeziu, P.S. Kuhn, A. Buck, T. Hofmann, C. Gerner, G. Hermann, G. Koellensperger , B. K. Keppler, W. Berger, P. Heffete, *Cancer Letters*, 2017, **404** , 79-88.

[41] C.G. Hartinger, P.J. Dyson, *Chem. Soc. Rev*., 2009, **38**, 391-401.

[42] P. Zhang, P. J. Sadler, *J. Organom. Chem*., 2017, **839**, 5-14.

[43] B.S. Murray, M.V. Babak, C.G. Hartinger, P.J. Dyson, *Coord. Chem. Rev.*, 2016, **306**, 86-114.

[44] G. Palermo, A. Magistrato, T. Riedel, T. von Erlach, C. A. Davey, P. J. Dyson, U. Rothlisberger, *Chem. Med. Chem*., 2016, **11**, 1199-1210.

[45] E. Păunescu, S. McArthur, M. Soudani, R. Scopelliti, P. J. Dyson. *Inorg. Chem*., 2016, **55**, 1788-1808.

[46] A. Ashraf, M. Hanif, M. Kubanik, T. Söhnel, S. M. F. Jamieson, A. Bhattacharyya, C. G. Hartinger, *J. Organom. Chem*., 2017, **839**, 31-37.

[47] Q. Ru, X. Tian, Y. X. Wu, R.H. Wu, M. S. Pi, C. Y. Li, *Oncol. Rep.*, 2014, **31**, 842-848.

[48] E. K. Hoffmann, I. H. Lambert, *Phil. Trans. R. Soc. B.*, 2014, **369,** 20130109.

[49] W. Wang, J. Xiao, M. Adachi, Z. Liu, J. Zhou, *Cell. Physiol. Biochem.*, 2011, **28**, 199-208.

[50] L. S. Chin, C. C. Park, K. M. Zitnay, M. Sinha, A. J. DiPatri, P. Perillán, J. M. Simard, *J. Neurosci. Res.*, 1997, **48**, 122-127.

[51] F. J. Al-Shammary, N. A. Aziz Mian, M. S. Mian, *Anal. Profiles Drug Subst. Excipients*, 1992, **21,** 345-373.

[52] T. M. K. Motawi, Y. Bustanji, S. EL-Maraghy, M. O. Taha, M. A. S. Al-Ghussein, *J. Enzym. Inhib. Med. Ch. ,* 2014, **29**, 153-161.

[53] M. S. Kim, J. E. Kim, D. Y. Lim, *Cancer Prev. Res.*, 2014, **7**, 236-245.

[54] J. Deb, J. Majumder, S. Bhattacharyya, S. S. Jana, *BMC Cancer,* 2014, **14**, 567-574.

[55] B. Tarusa, H. Bertrandb, G. Zeddab, C. D. Primoc, S. Quideaub, A. Slama-Schwok, *J. Biomol.Struct. Dyn.,* 2015, **33**, 1899-1912.

[56] Y. A. Ammar, M. A. Salem, Eman A. Fayed, M. H. Helal, M. S. A. El-Gaby, H. Kh. Thabeta, *Synthetic Commun.,* 2017, **47**, 1341-1367.

[57] K. C. Duggan, D. J. Hermanson, J. Musee, J. J. Prusakiewicz, J. L. Scheib, B. D. Carter, S. Banerjee, J. A. Oates, L. J. Marnett, *Nat. Chem. Biol.*, 2011, **7**, 803-809.

[58] M. S. Kim, J. E. Kim, D.Y. Lim, Z. Huang, H. Chen, A. Langfald, R. A. Lubet, C.J. Grubbs, Z. Dong, A.M. Bode, *Cancer Prev. Res.*, 2014, **7**, 236-245.

[59] V. Lhiaubet-Vallet, M.A. Miranda, *Pure Appl. Chem*., 2006, **78**, 2277-2286.

[60] D. E. Moore, P. P. Chappuis, *Photochem. Photobiol*., 1988, **47**, 173-180.

[61] P. Kuś, V. Kozik, M. Rojkiewicz, A. Sochanik, A. Szurko, M. Kempa, P. Kozub, M. Rams-Baron, K. Jarzembek, M. Stefaniak, J. Sakowicz, *Dyes Pigments*, 2015, **116**, 46-51.

[62] A. Catalfo, G. Bracchitta, G. De Guidi, *Photochem. Photobiol. Sci.*, 2009, **8**, 1467-1475.

[63] T. M. Georgiadis, M. M. Georgiadis, F. Diederich, *J. Org. Chem.*, 1991, **56**, 3362-3369.

[64] P. Mandal, B. K. Kundu, K. Vyas, V. Sabu, A. Helen, S. S. Dhankhar, C. M. Nagaraja, D. Bhattacherjee, K. P. Bhabake, S. Mukhopadhyay, *Dalton Trans.*, 2018, **47**, 517-527.

[65] M. A. Bennett, T. N. Huang, T. W. Matheson, A. K. Smith, J. P. Fackler, Jr., Ed., *Inorganic Syntheses* XXI, 1982, John Wiley & Sons, Inc., New York, vol. XXI, 74.

[66] J. Will, A. Kyas, W. S. Sheldrick, D. Wolters, *J. Biol. Inorg. Chem*., 2007, **12**, 883-894.

[67] S. Fery-Forgues, D. Lavabre, *J. Chem. Educ*., 1999, **76**, 1260-1264.

[68] L.J. Martínez, J.C. Scaiano, *Photochem. Photobiol*., 1998, **68**, 646-651.

[69] M.J. Frisch , G.W. Trucks, H.B. Schlegel, G.E. Scuseria, M.A. Robb, J.R. Cheesman, V.G. Zakrzewski, J.A. Montgomery Jr., R.E. Stratmann, J.C. Burant, S. Dapprich, J.M. Millam, A.D. Daniels, K.N. Kudin, M.C. Strain, O. Farkas, J. Tomasi, V. Barone, M. Cossi, R. Cammi, B. Mennucci, C. Pomelli, C. Adamo, S. Clifford, J. Ochterski, G.A. Petersson, P.Y. Ayala, Q. Cui, K. Morokuma, N. Roga, P. Salvador, J.J. Dannenberg, D.K. Malick, A.D. Rabuck, K. Raghavachari, J.B. Foresman, J. Cioslowski, J.V. Ortiz, A.G. Baboul, B.B.

Stefanov, G. Liu, A. Liashenko, P. Piskorz, I.Komaromi, R. Gomperts, R.L. Martin, D.J. Fox, T. Keith, M.A. Al-Laham, C.Y. Penng, A. Nanayakkara, M. Challacombe, P.M.W. Gill, B. Johnson, W. Chen, M.W. Wong, J.L. Andres, C. Gonzalez, M. Head-Gordon, E.S. Replogle, J.A. Pople, GAUSSIAN 09; Revision B02, Gaussian, Inc.: Pittsburgh, PA, 2003.

[70] J. P. Perdew, K. Burke, M. Ernzerhof, *Phys. Rev. Lett*., 1996, **77**, 3865-3868.

[71] C. Adamo, V. Barone, *J. Chem. Phys*., 1999, **110**, 6158-6170.

[72] L. E. Roy, P. J. Hay, R. L. Martin, *J. Chem. Theory Comput*., 2008, **4**, 1029-1031.

[73] T. H. Dunning Jr., *J. Chem. Phys*., 1989, **90**, 1007-1023.

[74] R. Krishnan, J. S. Binkley, R. Seeger, J. A. Pople, *J. Chem. Phys*., 1980, **72**, 650-654.

[75] Y. Zhao, N. E. Schultz, D. G. Truhlar, *J. Chem. Phys*., 2005, **123**, 161103.

[76] Y. Zhao, N. E. Schultz, D. G. Truhlar, *J. Chem. Theory Comput*., 2006, **2**, 364-382.

[77] Y. Zhao, D. G. Truhlar, *J. Chem. Phys*., 2006, **125**, 194101.

[78] Y. Zhao, D. G. Truhlar, *Theor. Chem. Acc*., 2008, **120**, 215-241.

[79] A. D. Boese, J. M. L. Martin, *J. Chem. Phys*., 2004, **121**, 3405-3416.

[80] A. D. Becke, *J. Chem. Phys*., 1993, **98**, 5648-5652.

[81] P. J. Stephens, F. J. Devlin, C. F. Chabalowski, M. J. Frisch, *J. Phys. Chem*., 1994, **98**, 11623-11627.

[82] S. Grimme, *J. Comp. Chem*., 2006, **27**, 1787-1799.

[83] J. P. Perdew, *Phys. Rev. B*, 1986, **33**, 8822-8824.

[84] J. D. Chai, M. Head-Gordon, *Phys. Chem. Chem. Phys.* 2008, **10**, 6615-6620.

[85] G. Scalmani, M. J. Frisch, *J. Chem. Phys*. 2010, **132**, 114110.

[86] I. Mayer, *Chem. Phys. Lett*., 1983, **97**, 270-274.

[87] K. B. Wiberg, *Tetrahedron*, 1968, **24**, 1083-1096.

[88] A. E. Reed, P.V.R. Schleyer, *Inorg. Chem*., 1988, **27**, 3969-3987.

[89] A. E. Reed, R. B. Weinstock, F. Weinhold, *J. Chem. Phys*., 1985, **83**, 735-746.

[90] E. D. Glendening, J. K. Badenhoop, A. E. Reed, J. E. Carpenter, J. A. Bohmann, C. M. Morales, F. Weinhold, NBO 6.0, Theoretical Chemistry Institute; University of Wisconsin: Madison, WI, 2013 (nbo6.chem.wisc.edu/).

[91] R. Bauernschmitt, R. Ahlrichs, *Chem. Phys. Lett*., 1996, **256**, 454-464.

[92] C. Van Caillie, R. D. Amos, *Chem. Phys. Lett*., 1999, **308**, 249-255.

[93] G. Scalmani, M. J. Frisch, B. Mennucci, J. Tomasi, R. Cammi, V. Barone, *J. Chem. Phys*., 2006, **124**, 94107.

[94] A. Juberta, M. L. Legartob, N. E. Massac, L. L. Tévez, N. B. Okulik, *J. Mol. Struc*., 2006, **783**, 34-51.

[95] D. A. Tocher, R. O. Gould, T. A. Stephenson, M. A. Bennett, J. P. Ennett, T. W. Matheson. *J. Chem. Soc. Dalton Trans*., **0**, 1983, 1571-1780.

[96] M. A. Bennett, J. P. Ennett, *Organometallics*, 1984, **3**, 1365-1374.

[97] J. C. S. Lopes, J. L. Damasceno, P. F. Oliveira, A. P. M. Guedes, D. C. Tavares, V. M. Deflon, N. P. Lopes, M. Pivatto, A. A. Batista, P. I. S. Maiag, G. Von Poelhsitz, *J. Braz. Chem. Soc*., 2015, **26**, 1838-1847.

[98] Nakamoto K. *Infrared and Raman spectra of inorganic and coordination compounds. Part B: Applications in coordination, organometallic and bioinorganic chemistry*, 5th ed. 1997, New York, John Wiley & Sons, Inc.

[99] R. B. Viana, A. R. Souza, B. S. Lima-Neto, A. B. F. Silva, *Polyhedron*, 2014, **81**, 661-667.

[100] M. Patra, T. Joshi, V. Pierroz, K. Ingram, M. Kaiser, S. Ferrari, B. Spingler, J. Keiser, G. Gasser, *Chem. Eur. J*., 2013, **19**, 14768-14772.

[101] A. B. Chaplin, P. J. Dyson, *J. Organom. Chem*., 2011, **696**, 2485-2490.

[102] L. Biancalana, A. Pratesi, F. Chiellini, S. Zacchini, T. Funaioli, C. Gabbiani, F. Marchetti, *New J. Chem*., 2017, **41**, 14574-14588.

[103] M. Melchart, A. Habtemariam, S. Parsons, S. A. Moggach, P. J. Sadler, *Inorg. Chim. Acta*, 2006, **359**, 3020–3028.

[104] F. Aman, M. Hanif, W. A. Siddiqui, A. Ashraf, L. K. Filak, J. Reynisson, T. Söhnel, S. M. F. Jamieson, C. G. Hartinger, *Organometallics*, **2014**, 33, 5546–5553.

[105] L. Biancalana, Guido Pampaloni, S. Z. Pratesi, F. Marchetti, *J. Organom. Chem*., 2018, **869**, 201-211.

[106] K. T. Prasad, B. Therrien, K.M. Rao, *J. Organomet. Chem*., 2010, **695**, 226-234.

[107] T. S. Morais, T. J. L. Silva, F. Marques, M. P. Robalo, F. Avecilla, P. J. A. Madeira, P. J. G. Mendes, I. Santos, M. H. Garcia, *J. Inorg. Biochem.*, 2012, **114**, 65-74.

[108] S. Dougan, M. Melchart, A. Habtemariam, S. Parsons, P. Sadler, *Inorg. Chem.*, 2006, **45**, 10882-10894.

[109] J. I. Aihara, *J. Phys. Chem. A*, 1999, **103**, 7487-7495.

[110] J. Palmucci, F. Marchetti, R. Pettinari, C. Pettinari, R. Scopelliti, T. Riedel, B. Therrien, A. Galindo, P. J. Dyson, *Inorg. Chem*., 2016, **55**, 11770-11781.

[111] F. Marchetti, R. Pettinari, C. Di Nicola, C. Pettinari, J. Palmucci, R. Scopelliti, T. Riedel, B. Therrien, A. Galindo, P. J. Dyson, *Dalton Trans.*, 2018, **47**, 868-878.

[112] X. Li, D. Zhang, G. Lu, G. Xiao, H. Chi, Y. Dong, Z. Zhang, Z. Hu, J. *Photochem. Photobiol. A Chem*., 2012, **241**, 1-7.

[113] M. Patra, G. Gasser, *Chem. Bio. Chem*., 2012, **13**, 1232-1252.

[114] F. Boscá, M.L. Marín, M. A. Miranda, *Photochem. Photobiol.* 2001, **74**, 637.

[115] H. Liu, F. X. Li, Y. Pi, D. J. Wang, Y. J. Hu, J. Zheng, *Spectrochim. Acta Part A Mol. Biomol. Spectrosc*., 2015, **145**, 588-593.

[116] K. S. Siddiqi, S. M. Bano, A. A. P. Ayaz Khan, *Chin. J. Chem*. 2009, **27**, 1755-1761.

[117] J. M. López-de-Luzuriaga, M. Monge, M.E. Olmos, D. Pascual, *J. Lumin*. 2014, **154**, 322-327.

[118] B. Albinsson, M. P. Eng, K. Pettersson, M. U. Winters, *Phys. Chem. Chem. Phys*. 2007, **9**, 5847-5864.

[119] E. A. Khramtsova, D. V. Sosnovsky, A. A. Ageeva, E. Nuin, M. L. Marin, P.A. Purtov, S. S. Borisevich, S. L. Khursan, H. D. Roth, M. A. Miranda, V. F. Plyusnin, T. V. Leshina, *Phys. Chem. Chem. Phys*. 2016, **18**, 12733-12741.

[120] I. Vayá, I. Andreu, M. C. Jiménez, M. A. Miranda, *Photochem. Photobiol. Sci*. 2014, **13**, 224-230.

[121] M. González-Béjar, E. Alarcón, H. Poblete, J. C. Scaiano, J. Pérez-Prieto, *Biomacromolecules*, 2010, **11**, 2255-2260.

[122] M. Van De Weert, *J. Fluoresc*., 2010, **20**, 625-629.

[123] Martin J. Stoddart (ed.), *Mammalian Cell Viability: Methods and Protocols*, Methods in Molecular Biology, 2011, vol. 740, Humana Press © Springer Science Business Media, LLC.

[124] P. Skehan, R. Storeng, D. Scudiero, A. Monks, J. McMahon, D. Vistica, J. T. Warren, H. Bokesch, S. Kenney, M. R. Boyd, *J. Natl. Cancer I.*, 1990, **82**, 1107-1112.

[125] Y. P. Keepers, P. E. Pizao, Godefridus J. Peters, J. van Ark-Otte, B. Winograd, H. M. Pinedo, *Eur. J. Cancer*, 1991, **27**, 897-991.

[126] Z. H. Lu, X. Gu, K. Shi, X. Li, D. Chen, L. Chen, *Arab. J. Chem.*, 2017, **10**, 624-630.

[127] E. Henriksson, E. Kjellén, P. Wahlberg, J. Wennerberg, J. Kjellström, *In Vitro Cell. Dev. Biol. Animal*, 2006, **42**, 320-323.

(1)

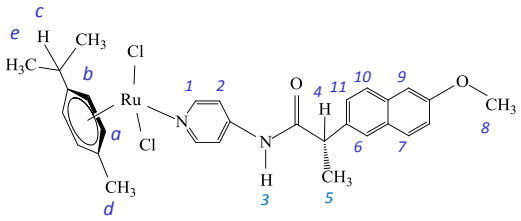

(2)

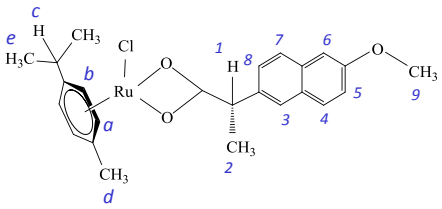

(3)

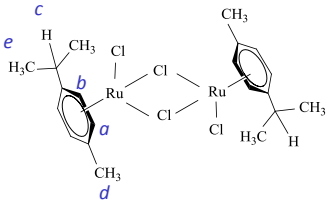

(4)

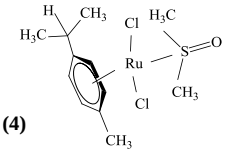

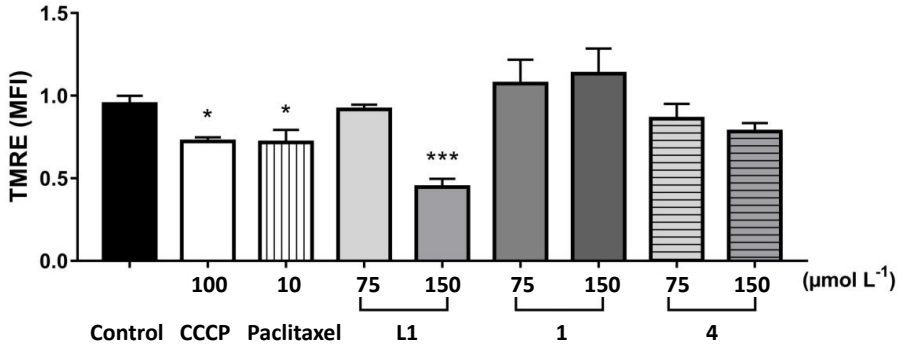

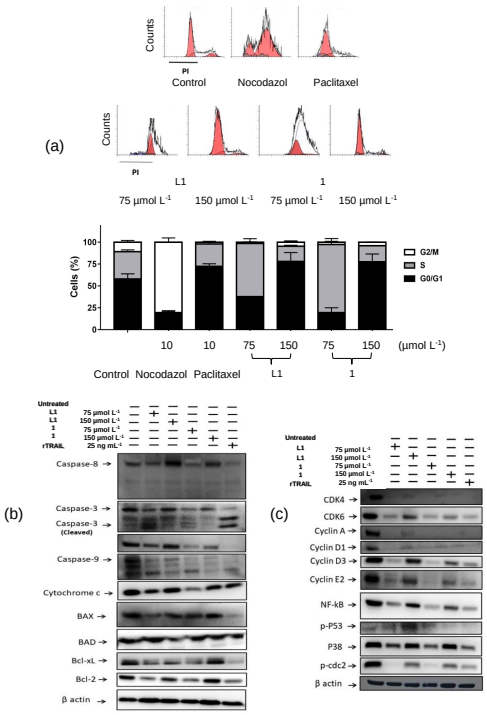

A new Ru(η^6-*p*-cymene) bearing the naproxen-pyridineamide (Npxpya) is synthesized and characterized by ESI-MS, NMR, ATR/FT-IR, UV/VIS and DFT computational calculations. Photophysical properties, antiproliferative activity, effects on mitochondrial membrane potential and cell cycle arrest in lung cancer cells are reported. All data are compared with those of Ru(II)-*p*-cymene-naproxenate, and the Npxpya and naproxen drugs.

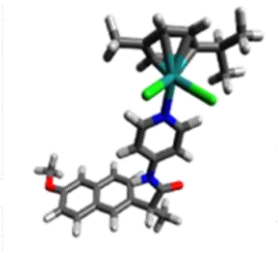

- The new Ru(II)-*p*-cymene bearing naproxen-pyridineamide (Npxpya) is synthesized
- Characterization is performed by ESI-MS, NMR, ATR/FT-IR, UV/VIS and DFT calculations
- Photophysical properties are described
- Antiproliferative activity, effects on mitochondrial membrane potential and cell cycle arrest in lung cancer cells are reported
- All data are compared with those of Ru(II)-*p*-cymene-naproxenate, and Npxpya and naproxen drugs